Design space for PEM electrolysis for cost-effective H_2 production using grid electricity

Doo Hyun Chung[1], Edward J. Graham[1], Benjamin Paren[2], Landon Schofield[3], Yang Shao-Horn[2,4,5], Dharik S. Mallapragada[1]

1. MIT Energy Initiative, Massachusetts Institute of Technology, Cambridge, MA
2. Research Laboratory of Electronics, Massachusetts Institute of Technology, Cambridge, MA
3. Department of Chemical Engineering, Massachusetts Institute of Technology, Cambridge, MA
4. Department of Mechanical Engineering, Massachusetts Institute of Technology, Cambridge, MA
5. Department of Materials Science and Engineering, Massachusetts Institute of Technology

ABSTRACT

Proton Exchange Membrane (PEM) electrolysis is a promising pathway for producing low-carbon hydrogen via electrolysis coupled with variable renewable energy (VRE). This study introduces a physics-based PEM electrolyzer model into an integrated design and scheduling optimization routine, allowing for a comprehensive evaluation of the impact of reactor level metrics (e.g., cathode pressure, current density) on the levelized cost of hydrogen (LCOH) across various cost, technology, and electricity supply scenarios. Benefits of static vs dynamic operation of PEM systems are outlined explicitly. The economic viability of a grid-based PEM electrolyzer producing 50,000 kg of hydrogen per day is assessed for both 2021 and 2035 technology scenarios. Results show that dynamic operation reduces the LCOH by 8% under the 2021 Scenario (4.98 to 4.57 \$/kg-H_2 at maximum current density 2 A/cm^2). Under 2035 price, cost and technology assumptions (maximum current density 4 A/cm^2), the LCOH ranges between 2.18-3.93 \$/kg-H_2 under static operation, and between 1.42-2.84 \$/kg-H_2 under dynamic operation, resulting in LCOH reductions of 20-50% depending on the electricity price profile. In addition, partial differential pressure mode with a cathode pressure of 5 bar was found to be the most cost-effective way to compress hydrogen to 30 bar in the 2021 Scenario, while full differential pressure mode is preferred in 2035 Scenarios. Finally, the study revealed that grid-based hydrogen production in 2021 does not meet the carbon intensity (CI) criteria for clean hydrogen in recent U.S. legislation, highlighting the need for dedicated renewable power sources for hydrogen electrolysis to qualify as "clean". These results suggest that capital cost reduction alone will not achieve low-cost electricity-based hydrogen production, emphasizing the need for further reductions in the cost of low-CI electricity to attain affordable and lower-carbon hydrogen production.

1. Introduction

The rapid expansion of renewable energy sources like wind and solar is necessary to combat climate change. A primary challenge, however, is managing the intermittent nature of such energy in a cost-effective manner. While commercially available Li-ion battery storage is becoming increasingly more cost-effective for storing energy over the period of hours, longer-term energy storage at scale remains challenging[1]. Hydrogen stands out as a promising low-carbon energy carrier that can provide a means of both long-term energy storage and long-distance energy transport, while serving as a vector for decarbonization end-uses where direct electrification remains challenging.

Among the various hydrogen production methods, electrolysis, whereby water is split into hydrogen and oxygen using electricity, offers a less carbon intensive alternative for producing hydrogen in comparison to steam methane reforming and autothermal reforming when driven by renewable power[2]. Current industrialized water electrolysis technologies for hydrogen production include alkaline and proton exchange membrane (PEM) electrolysis. While the alkaline process is more mature, PEM electrolysis is a particularly viable approach in this context, due to faster dynamical response times, wider current density range (0.1 – 6 A/cm^2 vs 0.1-0.4 A/cm^2 for alkaline[3]), reduced corrosion, and fewer components [3,4]. However, the current capital cost of PEM electrolysis remains a substantial hurdle, primarily due to membrane and electrocatalyst costs. This contributes the levelized cost of hydrogen (LCOH), which is estimated to be around \$5/kg to \$6/kg [5] . This cost is considerably higher than that of steam methane reforming (SMR), the most widely used industrial process for the generation of hydrogen, which ranges from approximately \$1.06/kg -\$1.64/kg [6]. [7]This cost disparity poses a major barrier to the widespread adoption of low-carbon electrolytic hydrogen. This disparity is diminishing however, due to substantial cost reductions in solar and wind electricity generation, as well as reductions in the upfront capital expenses related to electrolyzers [3,8,9].

Operating electrically driven processes dynamically in a variable renewable energy (VRE) dominated grid has the potential to drastically reduce operational expenditures, since the process can exploit surplus electricity during low-price periods (e.g., when supply exceeds demand). This approach presents an interesting optimization problem, since oversizing the system to deal with times of peak production leads to an increase in capital expenditure (CAPEX) and could increase the overall levelized cost of hydrogen. For electrochemical systems, an additional trade-off to consider is the decreased energy efficiency at high current densities due to increasing overpotentials [10]. Several studies have therefore considered the design and operations optimization of electrolyzer systems, with respect to time varying electricity prices. Roh et al. have formulated a total production cost minimization problem for a dynamically operating chlor-alkali electrolyzer [11]. Several techniques have been used to make the optimization problem tractable, including a) discretizing the time domain, b) using a piecewise linear approximation for the quadratic power demand function, and c) utilizing a golden-section search (GSS) decomposition method on the electrolyzer size, resulting in a series of mixed-integer linear programs (MILPs). Results have indicated that by oversizing a chlor-alkali electrolyzer and operating dynamically, the total production cost is reduced, provided that the specific capital costs of oversizing are low enough and the electricity price strongly fluctuates. Extending on the concept of oversizing electrolyzers to optimize the least-cost design, Mallapragada et al.[12] have developed a techno-economic optimization model to evaluate the economics of a photovoltaic (PV) PEM system, and have found system configurations and capital cost targets that result in LCOH that is competitive with hydrocarbon-based production methods [13]. In their work, location dependent H_2 storage and PV facilities were also

considered, and a simple model for the PEM electrolyzer was used, without explicitly modeling the polarization curve (current density – voltage dependence). Ginsberg et al. have considered the optimization of a PEM electrolyzer plants operating dynamically under California and Texas electricity price scenarios [3]. The study has considered various operation modes of the electrolyzer, highlighting the temporal variations in current density, ranging from minimum to maximum levels. Results indicated that dynamic operation reduces the LCOH by up to 63% for 2020 prices and by up to 53% for projected 2030 prices compared to static operation. Furthermore, operation above 2.5 A/cm^2 is justified at electricity prices below \$0.03/kWh. In their work, Ginsberg et al. [3] established a voltage-current density dependence in their model by regressing to three specific experimentally measured polarization curves, characterizing high, baseline and low electrolyzer efficiencies [14]. Our work aims to extend on the work of Ginsberg et al. [3] by modeling the PEM electrolyzer more predictively such that different design choices (e.g., electrolyzer pressure, and membrane thickness) may be readily analyzed within an integrated techno-economic optimization framework, without the extensive reliance on experimental data.

The previous literature on PEM electrolysis plants has focused on physics-based models [15,16] or dynamic operation optimization [3,12], but not considered both as part of a design and operations optimization framework. Studies using physics-based and cost models typically assess the LCOH under different operating conditions, identifying key drivers for cost reduction. For instance, Orella et. al have presented a generalized techno-economic model that can be used for various electrolytic processes and used it to evaluate the economics of PEM electrolysis [17]. In addition, Badgett et. al have provided a techno-economic assessment of the future production of hydrogen based on reduced capital cost as determined from a learning rate, manufacturing economies of scale, reduced material consumption, and improved electrolyzer performance [18]. Moreover, James et al. have provided a detailed techno-economic assessment (TEA) model specific to PEM systems, and conclude that the primary cost drivers are the electricity expenditures to run the electrolyzer and the capital cost of the electrolyzer [19]. Furthermore, Yates et. al have evaluated the potential of PV-PEM Electrolyzer systems using a Monte-Carlo approach to identify key drivers for reducing the LCOH [20]. Finally, Hancke et al. used a techno-economic model to evaluate the economics of differential-pressure operation of a PEM electrolyzer system by comparing the cost of direct electrochemical compression with the cost of mechanical compression [21].

The existing literature on PEM electrolysis plant, while comprehensive in several aspects, has important gaps that this work seeks to address. Previous studies have either focused on physics-based models, as seen in the works of [17–19], or on dynamic operation optimization[3,12,20,21]. However, most of these studies have not integrated both aspects: physics-based modeling and dynamic operation optimization with respect to process economics, within a single design and operations optimization framework. This integration is crucial for understanding the interplay between the physical properties of the electrolyzer and operation mode on its operational dynamics, especially under varying economic and environmental conditions. Our work builds on the above literature by: a) developing a physics-based PEM electrolyzer and TEA model that relates cell-level (e.g., membrane thickness) and plant parameters (e.g., operating temperature and pressure) with process economics, b) integrating the developed models as part of a techno-economic optimization framework considering dynamic operation, and c) considering a wide range of market scenarios such as region-specific electricity price profiles. The optimization framework allows for evaluating the cost-optimal design and scheduling of a commercial scale PEM electrolyzer plant connected to the grid with time-varying electricity prices and carbon intensities. We explicitly

characterize the CAPEX-OPEX tradeoff under dynamic and static operation and consider a limited treatment of the impact of differential pressure operation of the LCOH. Finally, our analysis considers the LCOH impacts of dynamic and static mode of operation considering today's grid as well as future renewables dominant power system with increased instances of zero-marginal cost electricity and price volatility.

2. Methodology

2.1. Electrolyzer Model

The electrolyzer model uses thermodynamic and electrochemical principles to generate a polarization curve, which describes the electrolyzer's voltage as a function of current density. The number of electrons transferred directly translates to the moles of products generated in an electrochemical reaction, so the polarization curve is a measure of voltage that is required to produce a unit mass of hydrogen. In this work, the polarization curve is calculated as the sum of the thermodynamic equilibrium voltage, ohmic overpotential, and activation overpotential for a given electrolyzer technology and design.

The thermodynamic equilibrium voltage necessary to create the chemical potential to drive the electrolysis process, also known as the open-circuit voltage, is given by the Gibbs Free Energy state equation combined with the Nernst Equation (Eq. S2). Using the state equations allows exploration of much wider temperature and pressure ranges than typical empirical or analytical expressions [16,22,23]. In this study, the model was used to evaluate the thermodynamic equilibrium voltage at an operating (cathode) pressure of 1 to 30 bar and an operating temperature of 80 °C. The ohmic resistance results from the resistances from the electron flow, proton flow, electrical contact in the membrane electrode assembly (MEA). The biggest contributor to the ohmic resistance in the PEM electrolyzer is the membrane [22,24]. Nafion 117 with a thickness of 178 um is assumed as the membrane technology for the current systems (2021 scenario) while thinner membranes (and thus lower ohmic resistance) is evaluated for the 2035 scenario (see Table 1).

The activation overpotential, also known as the kinetic overpotential, is the additional voltage that is needed to supply the activation energy to initiate the exchange of electrons in the electrochemical reactions [25,26]. The Butler-Volmer equation (Eq. S12) with the temperature-dependent exchange current density is used to calculate the activation overpotential as a function of current density.

Other models also include the concentration overpotential, which arises due to the overpopulation of reacting species near the electrodes interface. However, as long as the flow field is well designed for gas removal and the water circulation rate is high enough, the concentration overpotential can be neglected for PEM electrolysis [23,24,26–29]. For the purpose of making this model a computationally efficient techno-economic optimization tool, the thermal behavior of the electrolyzer was not modeled and it was assumed that an excess amount of water circulates through the system to provide the necessary cooling to control the operating temperature. In addition, the degradation of the electrolyzer stack was not modeled explicitly, but was accounted for in the TEA model by assuming regular refurbishment of the stack every 10 years. A detailed description of the electrolyzer model is available in SI1.

Figures 2a) and 2b) show that the electrolyzer model can be calibrated to make accurate predictions of experimental data [22,30] under various cell configurations and thermodynamic conditions. The model parameters for the 2021 and 2035 technology assumptions were chosen to match the performance of benchmark systems, including commercially available stacks, as shown in Figure S3.

a)

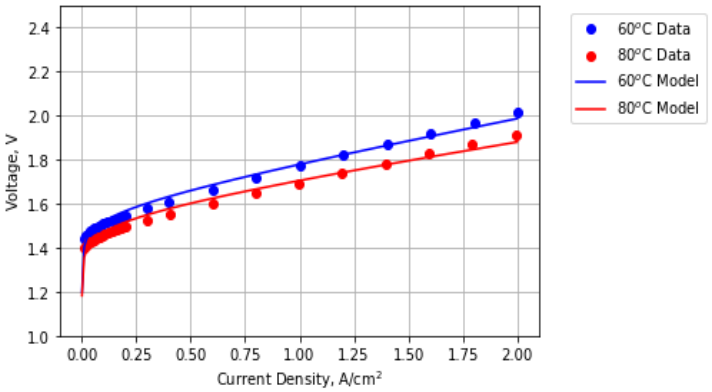

b)

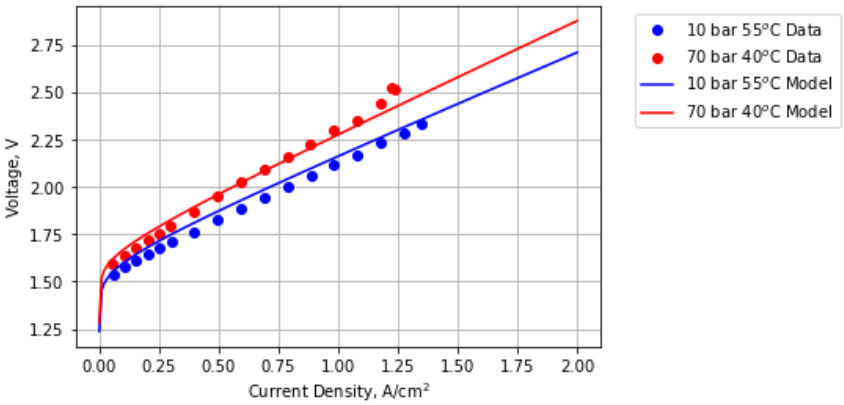

Figure 1: PEM polarization curves under varying thermodynamic conditions. a) Comparison of the electrolyzer model (line) with experimental data[30] (circles) at 80°C (red) and 60°C (blue) at ambient pressure. b) Comparison of the electrolyzer model (line) with experimental data[22] (circles) at (a) 55°C and 10 bar (blue); (b) 40°C and 70 bar (red).

2.2. Techno-Economic Analysis (TEA) Model

The TEA model used in this study was constructed by combining a physics-based PEM electrolyzer model with a system-level cost model for a PEM electrolyzer production plant shown in Figure 2. The production plant consists of the electrolyzer stack, the mechanical balance-of-plant, and the electrical balance-of-plant.

The electrolyzer plant cost model was adapted from the Department of Energy (DOE) H_2 A model [19], which is based on a detailed ASPEN-model based economic analysis and input from electrolyzer manufacturers. The resultant TEA model serves to determine the net present value (NPV) for the overall production facility, which is subsequently used as the objective function in the integrated design and scheduling optimization problem (see section 2.3).

a)

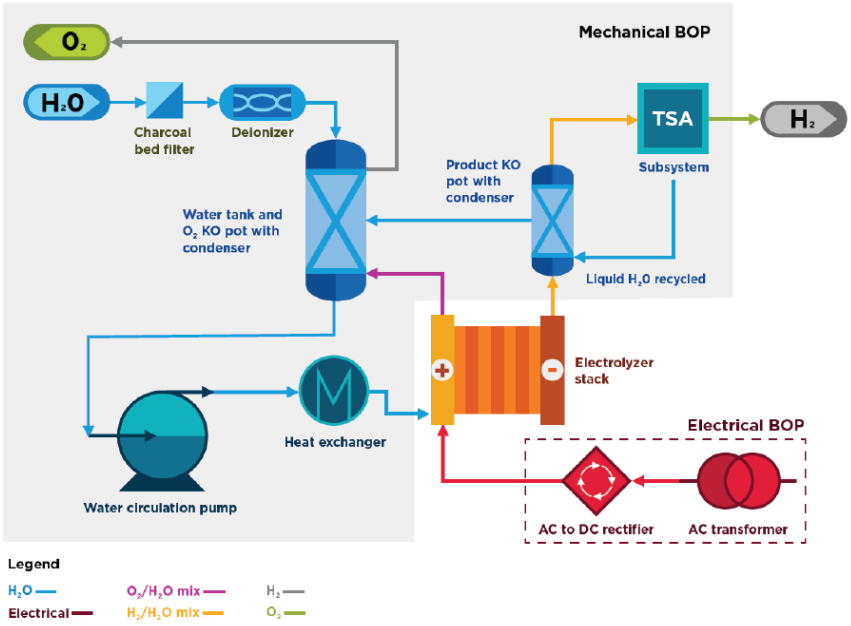

b)

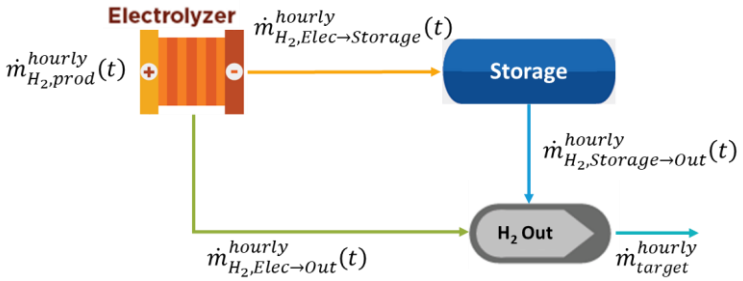

Figure 2: a) Schematic of the PEM electrolysis system showing the electrolyzer stack, the mechanical balance of plant, and the electrical balance of plant. Adapted from [31]. KO = Knock Out. b) Illustration of hydrogen flow paths from electrolyzer to storage to system outlet.

2.2.1. Electrolyzer Cost Model

The electrolyzer cost model was adapted from the Department of Energy (DOE)'s H_2 A model [19], which considers capital, operational, and overhead costs associated with different components of the electrolyzer plant, such as the stack, the mechanical balance-of-plant (BoP), and the electrical BoP. The stack cost was calculated based on the materials, labor, and capital costs associated with producing the stack. The mechanical BoP includes pumps, compressors, heat exchangers, water filtration system, knockout pots, and temperature swing adsorption system. The electrical BoP includes components such as transformers, rectifiers, switchgear, and control systems. The model also considers the cost of land, site preparation, and installation, as well as indirect costs such as project management, engineering, and contingency. The operational costs include the cost of electricity and feedwater that are necessary to operate the electrolyzer plant. To calculate the total cost of ownership of the electrolyzer plant, the net present value-calculation model was applied to the capital and operating costs over its expected lifespan. The model adopts the cost assumptions of the H_2 A model with modifications to adjust for inflation based on the Chemical Engineering Plant Cost Index (CEPCI) and for the 2021 reference dollar based on the U.S. Bureau of Economic Analysis's Consumer Price Deflator. A detailed description of the electrolyzer techno-economic model is available in SI3.

2.2.2. Compression Cost Model

For an electrolyzer plant whose target delivery pressure is 30 bar, the output hydrogen stream can be compressed electrochemically, mechanically, or a combination of both. The higher capital and operating expenses resulting from electrochemical compression were accounted for in the electrolyzer model through a pressure adjustment factor sourced from the literature (see Figures S4a and S4b), with the result that 15-bar stack has roughly a 20% higher capital cost than a stack at ambient conditions [32]. For mechanical compression, a separate cost model was developed using the Department of Energy's Hydrogen Delivery Scenario Analysis Model (HDSAM). The description of the compression model is provided in SI4.

2.3. Techno-Economic optimization framework

An optimization framework was formulated to ascertain the ideal plant sizing (specifically, the electrolyzer surface area and storage capacity), and optimal scheduling of the process-related operational variables (e.g., current density) over the course of year under time-varying electricity prices. The net present value of the plant cost was used as the objective function to be minimized. Since all scenarios considered in this work assume the same average daily production rate (see Section 2.5) this is equivalent to minimizing the LCOH. The LCOH was calculated by dividing the total discounted cost by the total discounted hydrogen production over the lifespan of the plant. The optimization problem was given by:

$$minimize\ NPV(C_{Total}) = minimize\ C_{CAPEX} + C_{storage} + \sum_{y=1}^{40}\left[\left(C_{PR} + C_{UPR} + C_{fOPEX} + C_{vOPEX}\right)\frac{(1+\pi)^y}{(1+d)^y}\right]. (1)$$

Where C_{CAPEX} is the capital expenditure ($), $C_{storage}$ is the capital expenditure for storage ($), C_{fOPEX} are the fixed operating expenses, C_{vOPEX} are the variable operating expenses, C_{PR} is the planned replacement cost, and C_{UPR} is the unplanned replacement cost. Throughout, we assume a plant lifetime of 40 years, an inflation rate (π) of 1.9%, and a discount rate adjusted for inflation (d) of 8%. The variable OPEX expenditures were determined by:

$$C_{vOPEX} = \sum_{d=0}^{364}\sum_{t=24d}^{24(d+1)-1} P_{elec}(t) \times Power_{op}\left(j_{op}(t)\right) + P_{elec}(t) \times U_{elec}^{hourly} \times \dot{m}_{H_2,prod}^{hourly}(t) + P_{water} \times U_{water}^{hourly} \times \dot{m}_{H_2,prod}^{hourly}(t). (2)$$

Where $P_{elec}(t)$ is the electricity price at time t, $Power_{op}\left(j_{op}(t)\right)$ is the electrolyzer stack power which is a function of current density ($j_{op}(t)$), U_{elec}^{hourly} and U_{water}^{hourly} are the hourly electrical usage and water usage respectively, and $\dot{m}_{H_2,prod}^{hourly}$ is the hourly mass flow of hydrogen produced. In equation (2), we sum over all hours of the year, and P_{elec} is a yearly electricity price profile, discretized in hours. Note that by substituting C_{vOPEX} in the NPV optimization (1), we assume that model dispatch over 1 year is duplicated over the other 39 years.

Under dynamic operation, a hydrogen storage device at the electrolyzer outlet (see Figure 1b) is modelled so that the system is allowed to store excess hydrogen during periods of low electricity prices and discharge it later, while meeting a fixed daily production rate. For simplicity, the storage can be charged or discharged, but not both at the same time. The storage model is described in more detail in SI6. A minimum current density limit for the electrolyzer is applied due to safety and efficiency considerations, and this is achieved via a big-M formulation (see SI Eqs S49 and S50). The optimization problem is discussed in more detail in SI6.

2.3.1. Solution method

Two techniques were used to make the optimization problem (1) numerically tractable. Firstly, due to the nonlinearities present in the electrolyzer model equations, a piecewise linear approximation was used to determine the stack power density as a function of current density (see SI6, SI Figure S24). This method improves optimization time and allows for implementation in Gurobi as the global optimization solver. Secondly, a golden section search (GSS) decomposition method is used to determine the optimal electrolyzer capacity (see SI6, and figures S23, S26 and S27), which results in the solution to many smaller MINLP subproblems with fixed electrolyzer capacity

The overall LCOH minimization problem is a mixed-integer linear program (MINLP), was implemented in Gurobi 9.5, and solved to a 1 % optimality gap. The optimization model consists of approximately 250,000 equations, 50,000 continuous variables and 60,000 binary variables. Typically, about 10 GSS iterations were required to reach a convergence tolerance of 1 tonne H_2/day (2% of the baseline value).

Since the electrolyzer capacity was fixed in the subproblem, the objective function in the inner loop of the GSS algorithm was simplified as:

$$minimize\ C_{storage} + \sum_{y=1}^{40}\left[C_{vOPEX}\frac{(1+\pi)^y}{(1+d)^y}\right] \quad (3)$$

Where $C_{storage}$ is the capital cost of the storage device, which increases linearly with storage inventory.

2.4. Grid electricity input data sources

In order to assess the impact of electricity price on the levelized cost of hydrogen (LCOH) in the 2021 Scenario, historical hourly locational marginal prices (LMP) from Southern California in 2021 [33] were used in the cost model. In addition, a typical grid interconnection cost of $0.03/W was added to the total electricity price.

For the 2035 scenario, multiple regional system electricity price projections for 2030-2040 from the National Renewable Energy Laboratory (NREL) 2021 Cambium Project [34] and the FLECCS Program [35,36] were used in the simulation. Brief descriptions of each of the electricity price scenarios used in this study are available in SI5.

2.5. Scenarios evaluated

Throughout this work, we employ a case study that uses grid electricity to supply 50,000 kg of H_2 per day, generated at an outlet pressure of 30 bar, in line with central, large, plant size H_2 production system described by [19]. The electrolyzer temperature is assumed to be 80 °C. The minimum operating current density, j_{min}, is assumed to be $0.5\ \mathrm{A/cm^2}$. The cathode and anode exchange current densities are assumed to be 2.3×10^{-3} and 3.0×10^{-6} A, respectively. Two modes of operation are considered: static and dynamic. Under static operations, the electrolyzer was constrained to operate at a constant nominal current density, producing a constant stream of hydrogen at the outlet. In this mode of operation, the electrolyzer plant was sized to exactly match the demand rate, thereby removing the need for a storage facility**.** In dynamic operations, the electrolyzer was allowed to vary the operating current density subject to technical and operational constraints. In addition, a storage facility is necessary to insulate the consumers from variable production of dynamic operations.

2.6. Cost and technology assumptions

A sensitivity study was carried out in order to assess the impact of different cost drivers on the LCOH. The sensitivity parameters include different technology, cost, and price assumptions on the basis of available calculations and projections in the literature. To ensure consistency in the assessment of plant costs, adjustments were made using the Chemical Engineering Plant Cost Index (CEPCI). This index accounts for changes in the costs of equipment, construction, and plant expenses, providing a reliable standard for evaluating the actual costs of the project. Additionally, all monetary figures were

standardized to 2021 values employing the Consumer Price Deflator. By converting all financial data to a common base year, this adjustment ensures a comparative analysis based on the prevailing economic conditions of 2021. Table 1 shows the electrolyzer model parameters assumed for the 2021 and 2035 Scenarios. Table 2 shows the cost model parameters assumed for the 2021 and 2035 Scenarios. In section 3.3 we also consider modifying the cathode pressure.

Table 1: Electrolyzer Model Parameters for various technology scenarios.

Parameter	2021 Scenario	2035 Scenario	Unit
Membrane Thickness	178[30]	127[10]	µm
Cathode Exchange Current Density	$2.3x10^{-3}$	$2.3x10^{-3}$	A/cm^2
Anode Exchange Current Density	$3.0x10^{-6}$	$3.0x10^{-6}$	A/cm^2
Temperature	80	80	°C
Cathode Pressure	30	30	Bar
Anode Pressure	1	1	Bar
Maximum or Nominal Current Density	1,2,3,4	4	A/cm^2
Minimum Current Density	0	0.5	A/cm^2

Table 2: Key technology cost assumptions across the two technology scenarios. See SI3 and SI4 for details. eBoP is the electrical balance of plant consists of an AC transformer to change the voltage of the AC power supply from the grid and a rectifier to convert the AC current to a DC current. The mechanical BoP (mBoP) consists of subsystems that perform secondary functions to support the electrolyzer stack [14].

Parameter	2021 Scenario	2035 Scenario	Unit
Electrolyzer Stack Cost	2	0.7	$\$/cm^2$
mBoP Cost	117	54	\$/(kg H_2 /day)
eBoP Cost	126	80	\$/kW electric
Total CAPEX	1,006	421	\$/kW input
Storage CAPEX	500	300	\$/kg
Grid interconnection cost	30		\$/kW
Discount rate for annualizing capital costs	8%		

3. Results And Discussion

In this study, we explore three main aspects that influence the LCOH for a PEM electrolysis plant: 1) static vs dynamic operational modes considering design and operational cost trade-offs, 2) system

design parameters like maximum current density and differential pressure operations and 3) the influence of different electricity price profiles and technology cost assumptions. We also include a brief discussion of the potential cost and design implications of the H_2 production tax credits available in the U.S. as part of the Inflation Reduction Act of 2022 with a more thorough discussion on this subject available elsewhere [37].

3.1. Impact of Dynamic vs Static Operations on LCOH Under 2021 Technology and Cost Assumptions

Under 2021 cost and technology assumptions noted in Table 1-2, dynamic operations reduce the LCOH by 5 - 11% compared to the equivalent static operations delivering the same hourly hydrogen production rate of 50 tonnes/day (Figure 3). The cost savings is attributed to the reducing variable operating costs (mostly power purchase costs), which account for up to 82% of the LCOH shown in Figure 3. Under dynamic operations, the cost-optimal electrolyzer dispatch results in increasing hydrogen production (by increasing current density) when the electricity is cheap and decreasing production when the electricity is expensive, as highlighted in temporal patterns in current density and electricity prices in Figure 4. By contrast, the electrolyzer in a static mode produces a constant stream of hydrogen by operating at a constant nominal current density of 2 A/cm^2 regardless of the fluctuations in the electricity prices.

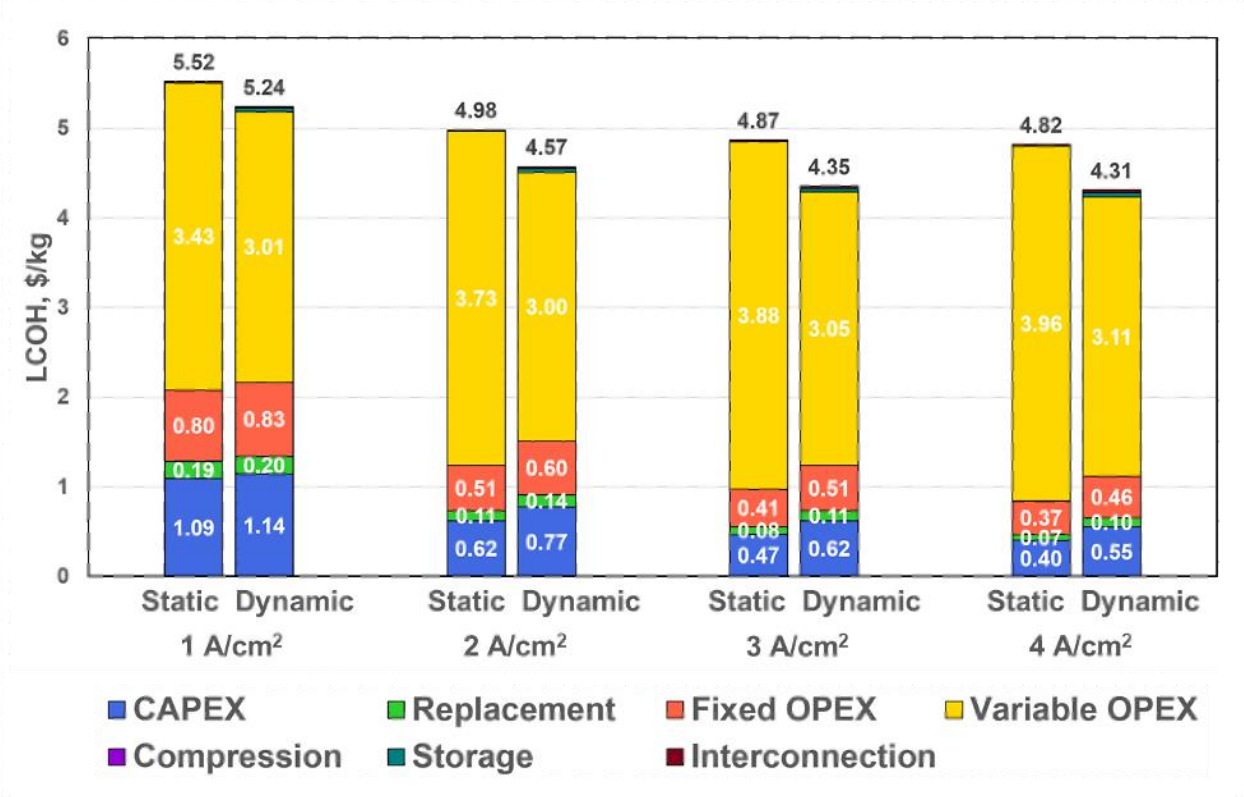

Figure 3: Optimized LCOH contributions under 2021 cost and technology assumptions. LCOH has units $/kg-$H_2$. For static operation, the current densities mentioned refer to the unchanging operation at the specified current density. Under dynamic operation, the current densities indicate the maximum permissible current density. The electrolyzer is given the flexibility to

operate below this maximum limit on an hourly basis. Electricity price scenario based on the historical data for node LAFRESA_6 in Southern California.

Although operational costs are lower under dynamic operation as compared to static operation, in order to achieve the same production target, the lower utilization rate in a dynamic mode was compensated with a larger production capacity (and thus greater fixed costs). For example, across the current density scenarios evaluated in Figure 3, the installed production capacity[†] is 4-38 % greater than the average H_2 production rate. Furthermore, investment in a compressed H_2 storage facility is necessary to buffer out the mismatch between a variable supply and a fixed H_2 demand. As shown in Figure 4, to compensate for this mismatch the electrolyzer produces more hydrogen at high current density and charges this to storage during low-price hours. During high price hours, hydrogen production is reduced by lowering current density and storage is discharged to meet the demand. There is also evidence of long-term hydrogen storage, where the longest continuous period where storage remains above 20% of the capacity is 46 days (starting on day 30). The incremental cost of H_2 storage in the dynamic operation case is relatively minor (< 2%) compared to the other variable and fixed costs of the electrolyzer, even while considering relatively expensive above-ground H_2 storage. The attractiveness of this approach is likely to increase if salt cavern-based H_2 storage, which has lower capital costs [38], becomes feasible.

Despite an increase in the electrolyzer nameplate capacity and the addition of the storage facility, the LCOH of dynamic operations is less than that of static operations. For the case study simulated for Southern California, oversizing the plant capacity by 33% with a nominal/maximum current density of 2 A/cm^2 led to an 8% decrease in LCOH, from 4.98 $/kg to 4.57 $/kg. Even with dynamic operation, the LCOH values in Figure 3 for current technology and grid conditions are still much greater than the cost of H_2 production from fossil options, which range between 0.5 - 1.7 $/kg, depending on natural gas prices (International Energy Agency, 2021). This gap suggests that further reductions in capital costs and electricity prices are needed to make H_2 production via PEM electrolyzers an economical option.

[†] The installed production capacity of the electrolyzer is evaluated at the maximum current density, which represents the upper limit on the hydrogen production rate. The calculation involves multiplying the maximum current density by the total cell area determined from the optimization algorithm, and applying Faraday's law to translate the electrical input into the mass flowrate of hydrogen (see SI Eq. 39)

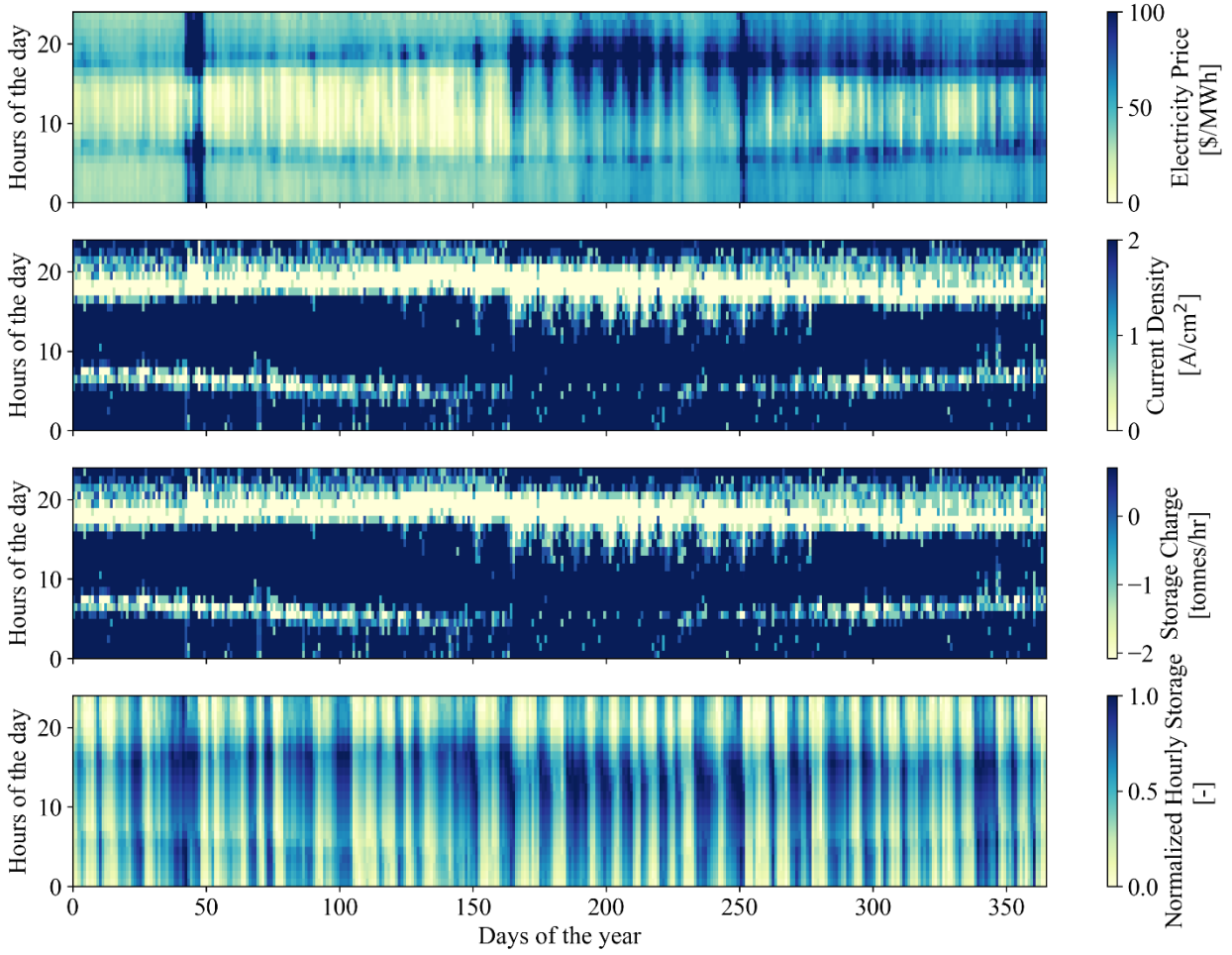

Figure 4: Optimal plant dispatch under 2021 cost and technology assumptions under dynamic operation. The electricity price corresponds to the LMP at the node LAFRESA_6 in Southern California. The maximum current density is set to 2A/cm². Negative values of storage charge refer to discharge.

Operating at a high current density is crucial to reducing the LCOH in both static and dynamic operational modes, enabling more hydrogen production per unit of cross-sectional area of electrolyzer cells, which in turn reduces the capital expenditure and other fixed costs associated with scaling the plant size (as depicted in Figure 3). Although variable operating expenses increase with increasing current density due to efficiency losses (see Figure 3), an overall cost reduction of 9.8% to 12.8% was achieved by increasing the current density from 1 A/cm^2 to 2 A/cm^2. The benefits of dynamic operations also increase with increasing current density. Since the cell is less efficient at higher current densities, a greater reduction in variable OPEX was achieved when the cell operates at part-loading. As shown in Figure 3, the LCOH is reduced by 5% at 1 A/cm^2, 8% at 2 A/cm^2, which is the typical limit of present systems, and 11% at both 3 and 4 A/cm^2 when transitioning from static to dynamic operations. A corollary observation from this result is that commercially alkaline electrolyzers that have much lower

current density ranges (typically around 0.1-0.4 A/cm^2) may be less valuable to exploit electricity price volatility for low-cost H_2 production as compared to PEM systems.

3.2. Impact of Electricity Price Profile on LCOH Under 2035 Technology and Cost Assumptions

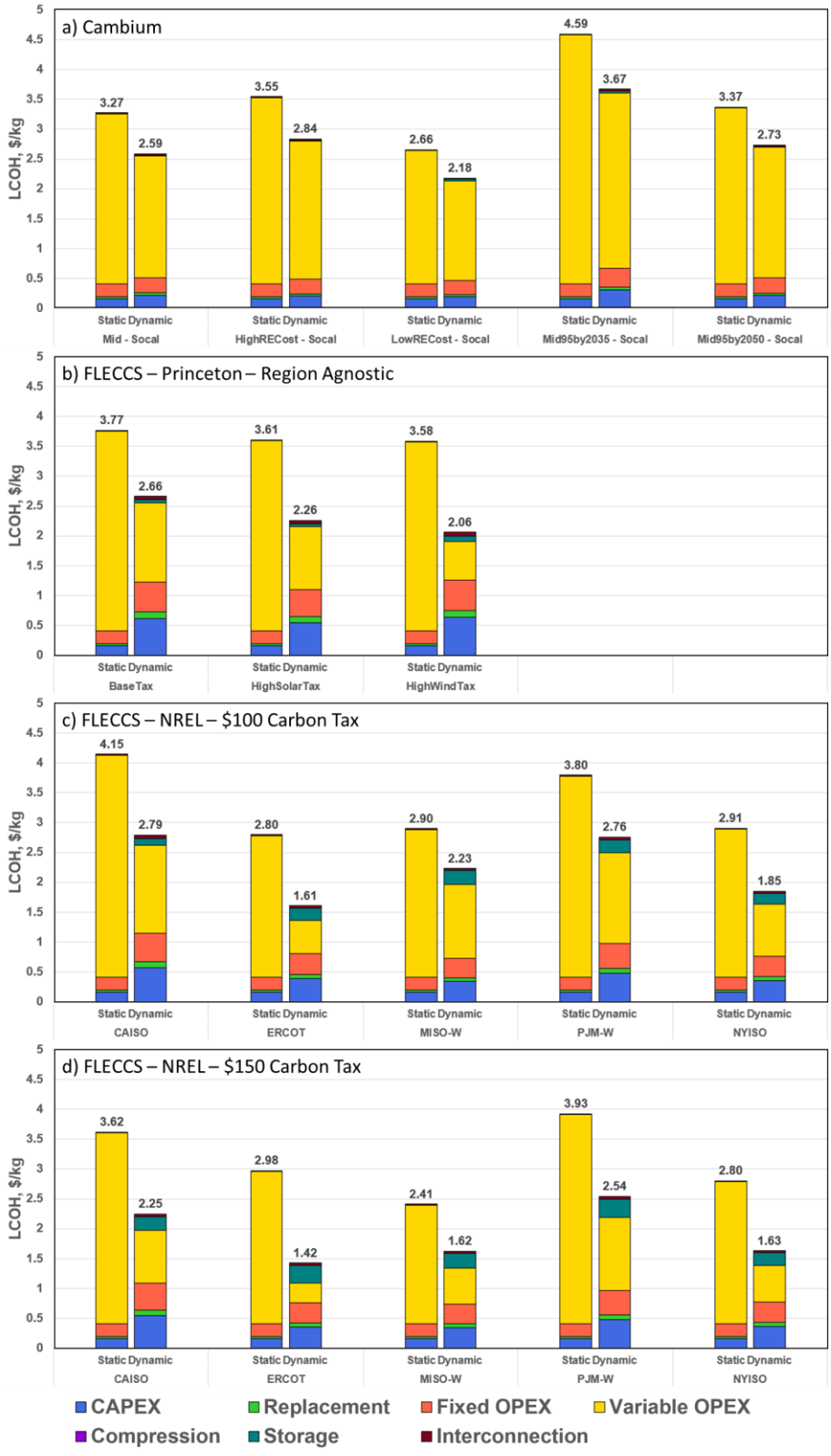

Figure 5 LCOHs with different electricity price projections with 2035 technology and cost assumptions. A nominal/maximum current density of 4 A/cm^2 is used for the static/dynamic operation scenarios. Each panel represent different set of electricity price scenarios retrieved from the literature. See further explanation on the price scenarios used here in section SI5.

Here we explore the LCOH impact of future projected cost and performance of electrolyzers and electricity price scenarios on the LCOH under static and dynamic operations. First, electrolyzers, particularly PEM systems, are relatively nascent technology, with global installed capacity at 90 MW as of 2020 [39]. Therefore, many studies expect that the capital costs for electrolyzers will significantly decrease in the future due to advancements in flow fields, membrane electrode assembly (MEA), labor, economies of scale, quality control, and larger cell areas [19,40,41]. Studies suggest that the learning rates for electrolyzers are comparable to those for solar PV, between 16% and 21% [42,43]. Additionally, IRENA 2020 predicts that a cost reduction of more than 40% can be achieved by 2030. With an annual decline rate of 4.8% [8], the cost of an electrolyzer stack is expected to decrease from 2.0 \$/cm^2 in 2021 to 0.7 \$/cm^2 in 2040. As the technology scales up, capital costs for balance-of-plant equipment are also expected to decrease, resulting in a total capital cost of \$421 /kW for the 2035 scenario (Table 2).

Second, technology improvements are expected to enhance the operational performance of electrolyzers. The development of thinner membranes and optimized catalyst layers can improve electrolyzer performance while also reducing the cost of the electrolyzer stack. While it is difficult to predict which technological advancements will be successful, it is anticipated that future electrolyzers will be able to use thinner membranes without compromising structural integrity and crossover resistance.

Third, as power costs are the biggest contributor to the total cost of electrolytic hydrogen production, we evaluated the impact of different future electricity price scenarios in order to understand the range of possible LCOH values under different grid contexts. As previously mentioned, the projections include 16 different hourly prices series forecasts for 2030-2040 from the NREL 2020 Cambium Scenarios [34] and the FLECCS Program [35,36]. The five NREL Cambium Scenarios use the Regional Energy Development System (ReEDS) model to simulate the electricity price series under different assumptions of renewable energy penetration (high/low renewable energy cost) and policy support (decarbonize 95% by 2035 or 2050). The price series data are obtained for 2040 in a balancing region corresponding to Southern California. In addition to the NREL Cambium Scenarios, the NREL price scenarios from the FLECCS program [35] also provide hourly price series data for 2035. These data are simulated with the reference natural gas prices from the EIA's Annual Energy Outlook study (AEO2020) and different carbon tax assumptions (\$100/tonne or \$150/tonne), for each of the major grid operators in the United States, including CAISO, ERCOT, MISO-W, NYISO, and PJM. In addition, the FLECCS Princeton data set offer region-agnostic hourly price series data for 2030, simulated with the assumptions of \$60/tonne carbon tax, AEO2020 REF natural gas prices, and mid/low costs for solar and wind clusters located across the country.

According to the simulation/optimization results depicted in Figure 5, dynamic operations become more valuable with future cost, technology, and electricity price assumptions. In comparison to the 5-11% reduction in the 2021 Scenario, dynamic operations in the 2035 Scenarios lead to a 20-50% reduction in LCOH from the equivalent static operations baselines. Oversizing plant capacity up to four times the target production rate enables this cost reduction. Oversizing plant capacity is advantageous due to several reasons. The future grid systems with more renewable power integration are expected to have higher price volatility (see section SI5 and Table S8 in SI), which provides more opportunities to

dynamically vary the electrolyzer power loads. Additionally, lower capital costs reduce the opportunity cost of oversizing the plant capacity.

Although there are clear benefits of dynamic operation, there are technical and operational challenges to be addressed to realize the full potential of dynamic operations as modeled in this study. For instance, hydrogen crossover from cathode to anode, which is likely to be more prevalent at lower current densities (near zero) may limit the duration up to which the electrolyzer can continue to operate low current densities. In addition, high-frequency cycling may limit the number of cycles due to degradation, and the response times of the balance-of-plant equipment may not be fast enough to exploit every trough in the price fluctuations. Nevertheless, the trend is clear that dynamic operations will play an increasingly important role in reducing the cost of hydrogen production in the future with lower capital costs, cheaper and more volatile electricity prices, and technological improvements.

Overall, Figure 5 shows that the cases simulated with an assumed capital cost of $421/kWe had an LCOH ranging from $1.4/kg to $3.6/kg, with an average of $2.5/kg, which is still higher than fossil-based production costs of $0.5/kg to $1.7/kg. We tested a bookend case where we adopted the electricity price scenario that resulted in the lowest LCOH (FLECCS MiNg_$150_ERCOT) and assumed a highly optimistic capital cost of $200/kW (see section SI7). This bookend case resulted in a LCOH of $1.20/kg (Figure S28). This finding suggests that reducing capital costs of existing technologies alone may not meet the U.S. Department of Energy's Hydrogen Shot target of $1/kg. It emphasizes the necessity for continued investments in low-cost renewable power and breakthrough technology research to achieve low-carbon and affordable hydrogen production.

3.3. Differential Pressure Operations

Most of the commercial electrolyzers available in 2021 come with a standard feature of 30 bar outlet pressure. Differential pressure operation is one way to achieve this, where the anodes remain at ambient pressure (1 bar), and the cathodes are pressurized to 30 bar. Another method is to carry out electrolysis at ambient pressure on both anode and cathode sides and then use mechanical compressors to pressurize the produced hydrogen. A hybrid solution is also possible, where the electrolysis occurs at an intermediate pressure on the cathode side, and the mechanical compressors then pressurize the hydrogen to the desired level. Under the modeled 2021 scenarios, we find that the operating at differential pressure is has minor impact on overall LCOH, with the most economical option being to operate cathode at 5 bar, as depicted in Figure 6. As the cathode pressure increases, the thermodynamic efficiency loss and higher pressure requirements increase operating expenses and capital costs. In comparison to ambient pressure operations, the increased operating expenses and capital costs required for differential pressure operation at 5 bar are more than offset by avoiding inefficient mechanical compression at low pressure ranges (compression ratio of 5 from 1 bar to 5 bar). Under the 2035 scenario, full electrochemical compression with a differential pressure of 30 bar is projected to be the most cost-effective mode of operation, eliminating the requirement for bulky and noisy mechanical compression systems. This is because the impact of higher pressure operation is mitigated by the lower average electricity price and electrolyzer capital costs.

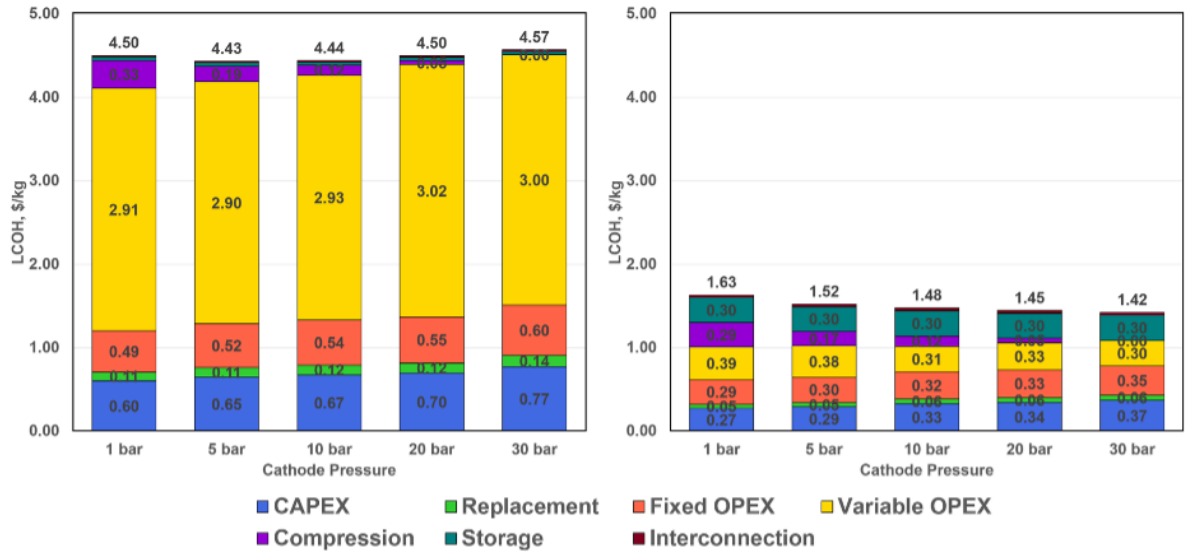

Figure 6: Optimized LCOH contributions under 2021 and 2035 cost and technology assumptions, with varying cathode pressures. Results correspond to dynamic operation. Left: LMP Southern California electricity price profile, maximum current density of 2 A/cm². Right: ERCOT electricity price profile, maximum current density of 4 A/cm².

3.4. Impact of the Inflation Reduction Act on LCOH

The Inflation Reduction Act (IRA) legislation in the U.S. introduces a 10-year production tax credit (PTC) mechanism under section 45V, based on the carbon intensity (CI) of the produced hydrogen as shown in Table 3. We examined whether any of the modeled scenarios align with the IRA's criteria, specifically exploring the carbon intensity (CI) thresholds for eligibility when accounting for embodied CI of grid electricity supply. Furthermore, we sought to explore strategies that could enable more effective utilization of the IRA's provisions, investigating potential avenues to optimize and fully capitalize on its benefits for hydrogen production.

Table 3: IRA 45V Production Tax Credit (PTC) by Hydrogen Production Carbon Intensity (CI).

Carbon Intensity (CI, kg CO_2/kg H_2)	Production Tax Credit (PTC, \$/kg H_2)
2.5 – 4	0.50
1.5 – 2.5	0.75
0.45 – 1.5	1.00
<0.45	3.00

For the 2021 scenario, the hydrogen CI was calculated using the average seasonal (quarterly) carbon emission intensity of the California grid system available at hourly resolution (annual average CI of 274

kg CO_2/MWh). Hourly carbon emissions were calculated by multiplying the CI with the electrolyzer power load. Then, the total carbon emissions are divided by the total mass of the produced hydrogen, which yields a CI of 13.18 kg CO_2/kg H_2. For the 2035 scenarios, the hourly marginal CI of the grid in Southern California is obtained from the NREL Cambium database. Under the Mid Scenario (average grid CI of 117 kg CO_2/MWh), the resulting hydrogen CI is 6.27 kg CO_2/kg H_2. In the 95% Decarbonization by 2050 Scenario (average grid CI of 146 kg CO_2/MWh), the CI stands at 7.78 kg CO_2/kg H_2. The 95% Decarbonization by 2035 Scenario (average grid CI of 18 kg CO_2/MWh) notably attains a CI of 0.79 kg CO_2/kg H_2, which underscores the critical need to reduce grid CI to minimize hydrogen CI. It reveals that only the most aggressive scenario, aiming for 95% decarbonization by 2035, manages to produce grid-based electrolytic hydrogen with a CI meeting the IRA standards, qualifying for \$1.00/kg H_2 assuming that the 45V PTC is still in effect by 2040.

The notable increase in PTC for the lowest CI bracket suggests a potential economic advantage in configuring the electrolyzer to follow the low-emissions grid hours, thereby reducing the hydrogen CI. We explored this scenario by adding a constraint in the optimization model to limit the CI of the produced hydrogen to not exceed 0.45 kg CO_2/kg H_2 in the case with electricity prices defined as per the 95% Decarbonization by 2035 Scenario. Implementing this constraint leads the optimization model to oversize the production capacity by 2.61 times the average H_2 demand, producing hydrogen at a CI of 0.43 kg CO_2/kg H_2. As can be seen in Table 4, this strategy leads to higher pre-PTC LCOH. However, the subsequent application of the PTC significantly reduces the post-PTC LCOH to below the post-PTC LCOH of the strictly pricing-following case without the emissions constraint. This result provides another illustration of the utility of dynamic operation in optimizing the long-term return on investment for a hydrogen production asset.

All the major U.S. grid systems in 2021 operate with a far higher CI (average of 379 kg CO_2/MWh) than what is necessary to qualify for the PTC credit, which implies that grid-connected electrolytic hydrogen production facilities that do not procure additional renewable power will not qualify for the PTC provisioned by the IRA. In other work, we have explored the emissions and cost impacts of alternative additionality and time-matching requirements being contemplated to implement the PTC policy [37].

Table 4: Electrolyzer production capacity, Carbon Intensity (CI), Pre-PTC LCOH, and Post-PTC LCOH of 2021 Baseline and 2040 Future Scenarios. The 10-year PTC is postprocessed by levelizing the annual PTC with a discount rate of 8% and an effective tax rate of 20%. Electrolyzer production capacity, defined as per footnote[†] and reported relative to the average H2 demand. The 2040 electricity price scenarios are sourced from the NREL cambium database [34] and correspond to the grid in Southern California.

Scenario	Assessment Year	Mode	Capacity	CI (kg CO_2/ kg H_2)	Pre-PTC LCOH (\$/kg)	Post-PTC LCOH (\$/kg)
2021 Base	2021	2A Dynamic	1.32x	13.18	4.57	4.57
Mid	2040	4A Dynamic	1.36x	6.27	2.59	2.59
Decarbonize 95% by 2050	2040	4A Dynamic	1.33x	7.78	2.73	2.73
Decarbonize 95% by 2035	2040	4A Dynamic	1.89x	0.79	3.67	3.22
Decarbonize 95% by 2035	2040	4A Dynamic + Emissions	2.61x	0.43	4.03	2.67

		intensity constraint (≤ 0.45 $kgCO_2/kgH_2$)				

4. Conclusions

In this study, a techno-economic optimization framework was developed to compute the LCOH of a PEM hydrogen production facility under various price, cost, and technology assumptions. The framework was used to evaluate the benefits of dynamic operations and differential pressure operations under various grid scenarios. The results showed that dynamic operations lowered the LCOH by 8% under the 2021 scenario and by 15-20% under the 2035 sensitivity scenarios, indicating that dynamic operations would become more advantageous in the future. Partial differential pressure mode with a cathode pressure of 5 bar was identified as the most cost-effective way to compress hydrogen to 30 bar under the 2021 Scenario, while a full differential pressure mode was preferred under the 2035 scenarios. The emissions analysis showed that grid-based hydrogen production in 2021 does not meet the CI criteria for the IRA 45V PTC. Thus, future hydrogen electrolysis projects in the next decade will require a dedicated renewable power source to take advantage of the PTC.

This study comes with some model limitations that should be factored when interpreting the findings and form the basis for future work. First, the absence of modeling hydrogen crossover could lead to an over-estimation of hydrogen production efficiency and under-estimation in LCOH. Second, the electrolyzer model does not incorporate an explicit model for membrane degradation, and it is anticipated that dynamic operations and high current densities could negatively impact the lifespan of the electrolyzer [3]. Although a stack replacement cost is incorporated in the TEA analysis, the model does not account for the variation of degradation with dynamic operation or current density. Lastly, the price-taker assumption used as part of the LCOH calculation might simplify market dynamics and neglect potential impacts on hydrogen pricing due to variations in supply and demand. Future studies should address these gaps to provide a more realistic evaluation of PEM production facilities.

5. Acknowledgements

The authors acknowledge funding from Analog Devices Inc. for supporting the research undertaken in this project.

6. References

(1) Huang, Y.; Li, J. Key Challenges for Grid-Scale Lithium-Ion Battery Energy Storage. *Adv Energy Mater* **2022**, *12* (48). https://doi.org/10.1002/aenm.202202197.

(2) IEA. *Comparison of the Emissions Intensity of Different Hydrogen Production Routes, 2021*; 2021.

(3) Ginsberg, M. J.; Venkatraman, M.; Esposito, D. V.; Fthenakis, V. M. Minimizing the Cost of Hydrogen Production through Dynamic Polymer Electrolyte Membrane Electrolyzer Operation. *Cell Rep Phys Sci* **2022**, *3* (6). https://doi.org/10.1016/j.xcrp.2022.100935.

(4) Guo, Y.; Li, G.; Zhou, J.; Liu, Y. Comparison between Hydrogen Production by Alkaline Water Electrolysis and Hydrogen Production by PEM Electrolysis. In *IOP Conference Series: Earth and Environmental Science*; 2019; Vol. 371. https://doi.org/10.1088/1755-1315/371/4/042022.

(5) Vicker, J.; Peterson, D.; Randolph, K. Cost of Electrolytic Hydrogen Production with Existing Technology. *Deparment of Energy of United Staes of America* **2020**.

(6) Lewis, E.; McNaul, S.; Jamieson, M.; Henriksen, M. S.; Matthews, H. S.; Shultz, T.; Skone, T. J.; Stevens, R. Comparison of Commercial State-Of-The-Art, Fossil-Based Hydrogen Production Technologies; 2023. https://doi.org/10.52202/066314-0029.

(7) Parkinson, B.; Tabatabaei, M.; Upham, D. C.; Ballinger, B.; Greig, C.; Smart, S.; McFarland, E. Hydrogen Production Using Methane: Techno-Economics of Decarbonizing Fuels and Chemicals. *Int J Hydrogen Energy* **2018**, *43* (5), 2540–2555. https://doi.org/10.1016/J.IJHYDENE.2017.12.081.

(8) Glenk, G.; Reichelstein, S. Economics of Converting Renewable Power to Hydrogen. *Nat Energy* **2019**, *4* (3). https://doi.org/10.1038/s41560-019-0326-1.

(9) Esposito, D. V. Membraneless Electrolyzers for Low-Cost Hydrogen Production in a Renewable Energy Future. *Joule*. 2017. https://doi.org/10.1016/j.joule.2017.07.003.

(10) Buttler, A.; Spliethoff, H. Current Status of Water Electrolysis for Energy Storage, Grid Balancing and Sector Coupling via Power-to-Gas and Power-to-Liquids: A Review. *Renewable and Sustainable Energy Reviews*. 2018. https://doi.org/10.1016/j.rser.2017.09.003.

(11) Roh, K.; Brée, L. C.; Perrey, K.; Bulan, A.; Mitsos, A. Optimal Oversizing and Operation of the Switchable Chlor-Alkali Electrolyzer for Demand Side Management. In *Computer Aided Chemical Engineering*; 2019; Vol. 46. https://doi.org/10.1016/B978-0-12-818634-3.50296-4.

(12) Mallapragada, D. S.; Gençer, E.; Insinger, P.; Keith, D. W.; O'Sullivan, F. M. Can Industrial-Scale Solar Hydrogen Supplied from Commodity Technologies Be Cost Competitive by 2030? *Cell Rep Phys Sci* **2020**, *1* (9), 100174. https://doi.org/10.1016/j.xcrp.2020.100174.

(13) Mallapragada, D. S.; Gençer, E.; Insinger, P.; Keith, D. W.; O'Sullivan, F. M. Can Industrial-Scale Solar Hydrogen Supplied from Commodity Technologies Be Cost Competitive by 2030? *Cell Rep Phys Sci* **2020**, *1* (9), 100174. https://doi.org/10.1016/J.XCRP.2020.100174.

(14) Mayyas, A.; Ruth, M.; Pivovar, B.; Bender, G.; Wipke, K.; Mayyas, A.; Ruth, M.; Pivovar, B.; Bender, G.; Wipke, K. Manufacturing Cost Analysis for Proton Exchange Membrane Water Electrolyzers. *National Renewable Energy Laboratory* **2019**, No. August.

(15) Song, G. H.; Meng, H. Numerical Modeling and Simulation of PEM Fuel Cells: Progress and Perspective. *Acta Mechanica Sinica/Lixue Xuebao* **2013**, *29* (3). https://doi.org/10.1007/s10409-013-0037-y.

(16) Millet, P. Fundamentals of Water Electrolysis. In *Electrochemical Power Sources: Fundamentals, Systems, and Applications Hydrogen Production by Water Electrolysis*; 2021. https://doi.org/10.1016/B978-0-12-819424-9.00002-1.

(17) Orella, M. J.; Brown, S. M.; Leonard, M. E.; Román-Leshkov, Y.; Brushett, F. R. A General Technoeconomic Model for Evaluating Emerging Electrolytic Processes. *Energy Technology* **2020**, *8* (11), 1900994. https://doi.org/10.1002/ENTE.201900994.

(18) Badgett, A.; Ruth, M.; James, B.; Pivovar, B. Methods Identifying Cost Reduction Potential for Water Electrolysis Systems. *Curr Opin Chem Eng* **2021**, *33*, 100714. https://doi.org/10.1016/J.COCHE.2021.100714.

(19) James, B.; Colella, W.; Moton, J.; Saur, G.; Ramsden, T. PEM Electrolysis H2A Production Case Study Documentation. *PEM Electrolysis H2A Production Case Study Documentation* **2013**, No. December.

(20) Yates, J.; Daiyan, R.; Patterson, R.; Egan, R.; Amal, R.; Ho-Baille, A.; Chang, N. L. Techno-Economic Analysis of Hydrogen Electrolysis from Off-Grid Stand-Alone Photovoltaics Incorporating Uncertainty Analysis. *Cell Rep Phys Sci* **2020**, *1* (10), 100209. https://doi.org/10.1016/J.XCRP.2020.100209.

(21) Hancke, R.; Holm, T.; Ulleberg, Ø. The Case for High-Pressure PEM Water Electrolysis. *Energy Convers Manag* **2022**, *261*, 115642. https://doi.org/10.1016/J.ENCONMAN.2022.115642.

(22) Marangio, F.; Santarelli, M.; Calì, M. Theoretical Model and Experimental Analysis of a High Pressure PEM Water Electrolyser for Hydrogen Production. *Int J Hydrogen Energy* **2009**, *34* (3). https://doi.org/10.1016/j.ijhydene.2008.11.083.

(23) Awasthi, A.; Scott, K.; Basu, S. Dynamic Modeling and Simulation of a Proton Exchange Membrane Electrolyzer for Hydrogen Production. *Int J Hydrogen Energy* **2011**, *36* (22). https://doi.org/10.1016/j.ijhydene.2011.03.045.

(24) Biaku, C. Y.; Dale, N. V.; Mann, M. D.; Salehfar, H.; Peters, A. J.; Han, T. A Semiempirical Study of the Temperature Dependence of the Anode Charge Transfer Coefficient of a 6 KW PEM Electrolyzer. *Int J Hydrogen Energy* **2008**, *33* (16). https://doi.org/10.1016/j.ijhydene.2008.06.006.

(25) Bessarabov, D.; Millet, P. *PEM Water Electrolysis*; Pollet, B., Ed.; Academic Press, 2018; Vol. 1.

(26) Abdol Rahim, A. H.; Tijani, A. S.; Kamarudin, S. K.; Hanapi, S. An Overview of Polymer Electrolyte Membrane Electrolyzer for Hydrogen Production: Modeling and Mass Transport. *Journal of Power Sources*. 2016. https://doi.org/10.1016/j.jpowsour.2016.01.012.

(27) Choi, P.; Bessarabov, D. G.; Datta, R. A Simple Model for Solid Polymer Electrolyte (SPE) Water Electrolysis. In *Solid State Ionics*; 2004; Vol. 175. https://doi.org/10.1016/j.ssi.2004.01.076.

(28) Görgün, H. Dynamic Modelling of a Proton Exchange Membrane (PEM) Electrolyzer. *Int J Hydrogen Energy* **2006**, *31* (1). https://doi.org/10.1016/j.ijhydene.2005.04.001.

(29) Yigit, T.; Selamet, O. F. Mathematical Modeling and Dynamic Simulink Simulation of High-Pressure PEM Electrolyzer System. *Int J Hydrogen Energy* **2016**, *41* (32). https://doi.org/10.1016/j.ijhydene.2016.06.022.

(30) Liso, V.; Savoia, G.; Araya, S. S.; Cinti, G.; Kær, S. K. Modelling and Experimental Analysis of a Polymer Electrolyte Membrane Water Electrolysis Cell at Different Operating Temperatures. *Energies (Basel)* **2018**, *11* (12). https://doi.org/10.3390/en11123273.

(31) Peterson, D.; Vickers, J.; Desantis, D. DOE Hydrogen and Fuel Cells Program Record: Hydrogen Production Cost From PEM Electrolysis 2019. *DOE Hydrogen and Fuel Cells Program Record* **2020**.

(32) Saba, S. M.; Müller, M.; Robinius, M.; Stolten, D. The Investment Costs of Electrolysis – A Comparison of Cost Studies from the Past 30 Years. *International Journal of Hydrogen Energy*. 2018. https://doi.org/10.1016/j.ijhydene.2017.11.115.

(33) *www.caiso.com*.

(34) Gagnon, P.; Frazier, W.; Cole, W.; Hale, E. *Cambium Documentation: Version 2021*; 2021.

(35) Cohen, S.; Durvasulu, V. *NREL Price Series Developed for the ARPA-E FLECCS Program*; 2021.

(36) Jesse D Jenkins, S. C. Summary Report of the GenX and PowerGenome Runs for Generating Price Series (for ARPA-E FLECCS Project). Zenodo 2021. https://doi.org/10.5281/ZENODO.5765798.

(37) Cybulsky, A.; Giovanniello, M.; Schittekatte, T.; Mallapragada, D. S.; Initiative, M. I. T. E. Producing Hydrogen from Electricity: How Modeling Additionality Drives the Emissions Impact of Time-Matching Requirements. MIT Energy Initiative 2023.

(38) Papadias, D. D.; Ahluwalia, R. K. Bulk Storage of Hydrogen. *Int J Hydrogen Energy* **2021**, *46* (70). https://doi.org/10.1016/j.ijhydene.2021.08.028.

(39) International Energy Agency. *Global Hydrogen Review 2021 – Analysis - IEA*. Global Hydrogen Review.

(40) Schmidt, O.; Gambhir, A.; Staffell, I.; Hawkes, A.; Nelson, J.; Few, S. Future Cost and Performance of Water Electrolysis: An Expert Elicitation Study. *Int J Hydrogen Energy* **2017**, *42* (52). https://doi.org/10.1016/j.ijhydene.2017.10.045.

(41) Escobar-Yonoff, R.; Maestre-Cambronel, D.; Charry, S.; Rincón-Montenegro, A.; Portnoy, I. Performance Assessment and Economic Perspectives of Integrated PEM Fuel Cell and PEM Electrolyzer for Electric Power Generation. *Heliyon* **2021**, *7* (3). https://doi.org/10.1016/j.heliyon.2021.e06506.

(42) IRENA. *Green Hydrogen Cost Reduction: Scaling up Electrolysers to Meet the 1.5 ℃ Climate Goal*; 2020.

(43) Lagadec, M. F.; Grimaud, A. Water Electrolysers with Closed and Open Electrochemical Systems. *Nature Materials*. 2020. https://doi.org/10.1038/s41563-020-0788-3.

Design space for PEM electrolysis for cost-effective H_2 production using grid electricity – Supplementary Information

Doo Hyun Chung[1], Edward J. Graham[1], Benjamin Paren[2], Landon Schofield[3], Yang Shao-Horn[2,4,5], Dharik S. Mallapragada[1]

1. MIT Energy Initiative, Massachusetts Institute of Technology, Cambridge, MA
2. Research Laboratory of Electronics, Massachusetts Institute of Technology, Cambridge, MA
3. Department of Chemical Engineering, Massachusetts Institute of Technology, Cambridge, MA
4. Department of Mechanical Engineering, Massachusetts Institute of Technology, Cambridge, MA
5. Department of Materials Science and Engineering, Massachusetts Institute of Technology

SI1: Electrolyzer Model

The electrolyzer model summarizes the relationship between cell voltage and cell current based on the electrochemical principles. It considers the open-circuit voltage, activation overpotential, and ohmic overpotential to calculate the cell voltage that is required to drive electrochemical reactions in an electrolytic cell as shown in (Eq. S1).

$$V = E + \eta_{ohm} + \eta_{act} \quad \text{(Eq. S1)}$$

E is the thermodynamic equilibrium voltage, or open-circuit voltage, that is required to create the chemical potential that drives the hydrogen generation process. The thermodynamic equilibrium voltage can be derived from Gibbs free energy:

$$E = -\frac{\Delta G}{nF} \quad \text{(Eq. S2)}$$

Based on the stoichiometry of the overall reaction, ΔG can be expressed as follows:

$$\Delta G = G_{H_2}(T_{cat}, P_{cat}) + \frac{1}{2} G_{O_2}(T_{an}, P_{an}) - G_{H_2O}(T_{an}, P_{an}) \quad \text{(Eq. S3)}$$

Since $G = H - TS$, $H(T,P)$ and $S(T,P)$ can be used to calculate $G(T,P)$ for each species. For water, the enthalpy and entropy of formation can be obtained from the steam tables. For the gas molecules, an analytical method computes $G(T,P)$ by making temperature corrections on G in standard conditions and then making corrections for the pressure. The temperature dependence of enthalpy can be expressed as the following empirical model [1]:

$$H(T,1\ bar) - H(298\ K,1\ bar) = a(T - T_0) + \frac{b}{2}10^{-3}(T^2 - T_0^2) - c10^5\left(\frac{1}{T} - \frac{1}{T_0}\right) - \frac{e}{2}10^8\left(\frac{1}{T^2} - \frac{1}{T_0^2}\right) \quad \text{(Eq. S4)}$$

Similarly, the temperature dependence of entropy can be expressed as the following [1]:

$$S(T,1\ bar) - S(298\ K,1\ bar) = a(LnT - LnT_0) + b10^{-3}(T - T_0) - \frac{c}{2}10^5\left(\frac{1}{T^2} - \frac{1}{T_0^2}\right) - \frac{e}{3}10^8\left(\frac{1}{T^3} - \frac{1}{T_0^3}\right) \quad \text{(Eq. S5)}$$

The coefficients for the gas molecules are provided in Table S1 [1]:

Table S1: Coefficients for Hydrogen and Oxygen for Temperature Correction

Molecules	a	b	c	e
H_2 (g)	26.57	3.77	1.17	–
O_2 (g)	34.35	1.92	-18.45	4.06

Since the values of H and S are known at standard temperature and pressure (298K and 1 bar), $H(T,1\ bar)$, S$(T,1\ bar)$, and G$(T,1\ bar)$ can be calculated for any temperature T and 1 bar. Then, another analytical expression using the Virial expansion is used to describe the pressure dependence of G [1]:

$$G(T,P) - G(T,1\ bar) = RTLnP + BP + \frac{C - B^2}{2RT}P^2 \quad \text{(Eq. S6)}$$

where

$$B = b_1 + \frac{b_2}{T}\ (cm^3 mol^{-1}) \quad \text{(Eq. S7)}$$

$$C = c_1 + \frac{c_2}{T^{\frac{1}{2}}}\ (cm^3 mol^{-1}) \quad \text{(Eq. S8)}$$

The Virial coefficients for the gas molecules for pressure up to 1000 atm are given in Table S2 [1].

Table S2: Virial Coefficients for Hydrogen and Oxygen for Pressure Correction

Molecules	b1	b2	c1	c2
H_2 (g)	20.5	-1,857	-351	12,760
O_2 (g)	42.6	-17,400	-2,604	61,457

This two-step procedure of 1) correcting for temperature (Eq. S4 - S5) and then 2) correcting for pressure (Eq. S6 - S8) calculates G for each species at any temperature and pressure within the valid ranges of correlations (T < 100C, P < 1000 atm). Then, Eq. S3 is used to calculate ΔG and Eq. S2 to calculate E.

η_{ohm} is the ohmic overpotential which arises from the resistances from the electron flow, proton flow, electrical contact in the membrane. The biggest contributor to the ohmic resistance in the PEM electrolyzer is the membrane [2,3]. The area-dependent resistance of a membrane is given by the formula:

$$R_{membrane} = \frac{t}{\sigma_{mem}} \quad \text{(Eq. S9)}$$

where t is the thickness of the membrane and σ_{mem} is the conductivity of the membrane. The membrane conductivity is given by empirical correlations as shown below [4,5]:

$$\lambda_m = 0.043 + 17.81a_{H_2O} - 39.85a_{H_2O}^2 + 36a_{H_2O}^3 \quad \text{(Eq. S10)}$$

$$\sigma_{mem} = (0.00514\lambda_m - 0.00326)e^{\left(1268\left(\frac{1}{303}-\frac{1}{T}\right)\right)} \quad \text{(Eq. S11)}$$

where λ_m is the water hydration factor. Since the membrane is fully immersed in water during electrolytic operations [6,7], a_{H_2O} is assumed to be 1. According to Eq. S11, the membrane conductivity increases with increasing temperature, but it is not affected by changes in pressure.

η_{act} is the activation overpotential that is needed to supply the activation energy to initiate the exchange of electrons [5,8]. The Butler-Volmer equation, which is a commonly-used model for water electrolysis, describes the relationship between current density and activation overpotential [8]:

$$j = j_0 \left[exp\left(\frac{-\alpha_1 F z \eta_a}{RT}\right) - exp\left(\frac{\alpha_2 F z \eta_a}{RT}\right)\right]$$

(Eq. S12)

where j_0 is the exchange current density, α is the charge transfer coefficient, and η_a is the activation overpotential. Assuming that $\alpha = \alpha_1 = \alpha_2$, (Eq. S12) can be simplified to the following equation using the hyperbolic sine function:

$$\eta_a = \frac{RT}{\alpha z F}\left(\frac{j}{2j_0}\right)$$

(Eq. S13)

Previous studies have reported experimental values for the anode charge transfer coefficient and cathode charge transfer coefficient as 2 and 0.5, respectively [2–4,7,9–11]. However, the theoretical value for a charge transfer coefficient is between 0 and 1.

The exchange current density, j_0, is an intensive physical property that measures the ease with which the charge transfer occurs (Millet 2015, Chapter 2). It is a function of the physical characteristics of the electrolyte such as material and morphology, catalyst, age, and operating conditions [7,12]. For the Pt catalyst in the cathode, j_0 of 10^{-4}-10^{-3} A/cm^2 has been suggested [13,14]. For the Ir and Pt-Ir catalyst in the anode, j_0 of 10^{-13}-10^{-6} A/cm^2 has been used [3,13].

In this study, an approach from [7,15,16] is adopted to express the temperature dependence of j_0:

$$j_0 = j_0^{ref} exp\left[\frac{E_{act}}{R}\left(\frac{1}{T^{ref}} - \frac{1}{T}\right)\right]$$

(Eq. S14)

where j_0^{ref} is the reference exchange current density at the reference temperature, T^{ref}, and E_{act} is the activation energy corresponding to the OER (in the anode) or HER (in the cathode). The values of j_0^{ref} and E_{act} are summarized in Table S3.

Table S3: Values of Reference Current Density and Activation Energy for OER and HER

Variable	Value	Units	Reference
$j_{0,cathode}^{ref}$	0.75×10^{-3}	A/cm^2	[7,15,16]
$E_{act,cathode}$	30,000	J/mol	[17]
$j_{0,anode}^{ref}$	1.0×10^{-7}	A/cm^2	(Carmo et al., 2013; Coutanceau et al., 2018; García-Valverde et al., 2012)
$E_{act,anode}$	90,000	J/mol	[7,18]
T^{ref}	318	K	[7]

Therefore, the total activation overpotential of an electrolytic cell is:

$$\eta_a = -\frac{RT}{F}\left(\frac{j}{2j_{0,anode}}\right) + -\frac{RT}{F}\left(\frac{j}{2j_{0,cathode}}\right) \quad \text{(Eq. S15)}$$

SI2: Electrolyzer Model Validation

The electrolyzer model is validated by benchmarking the model with two experiments that were conducted in different operating conditions. In the first benchmarking experiment [12] a single-cell electrolyzer with Nafion 117 (membrane thickness of 178 µm) was tested at two different temperatures (60°C and 80°C) at ambient pressure. was used. Table S4 summarizes the parameters that were used in the model.

Table S4: Electrolyzer Model Parameters for Single-Cell Experiment at 60°C and 80°C

Parameters	Values	Units
Membrane Thickness, t	178	µm
Electrodes and Plates Resistance, R_{elec}	0	ohms
Temperature, T	60 and 80	°C
Cathode Pressure, P_{cat}	1	bar
Anode Pressure, P_{an}	1	bar

Figure S1 shows that the model predictions and experimental data match well for both the 60°C and 80°C experiments.

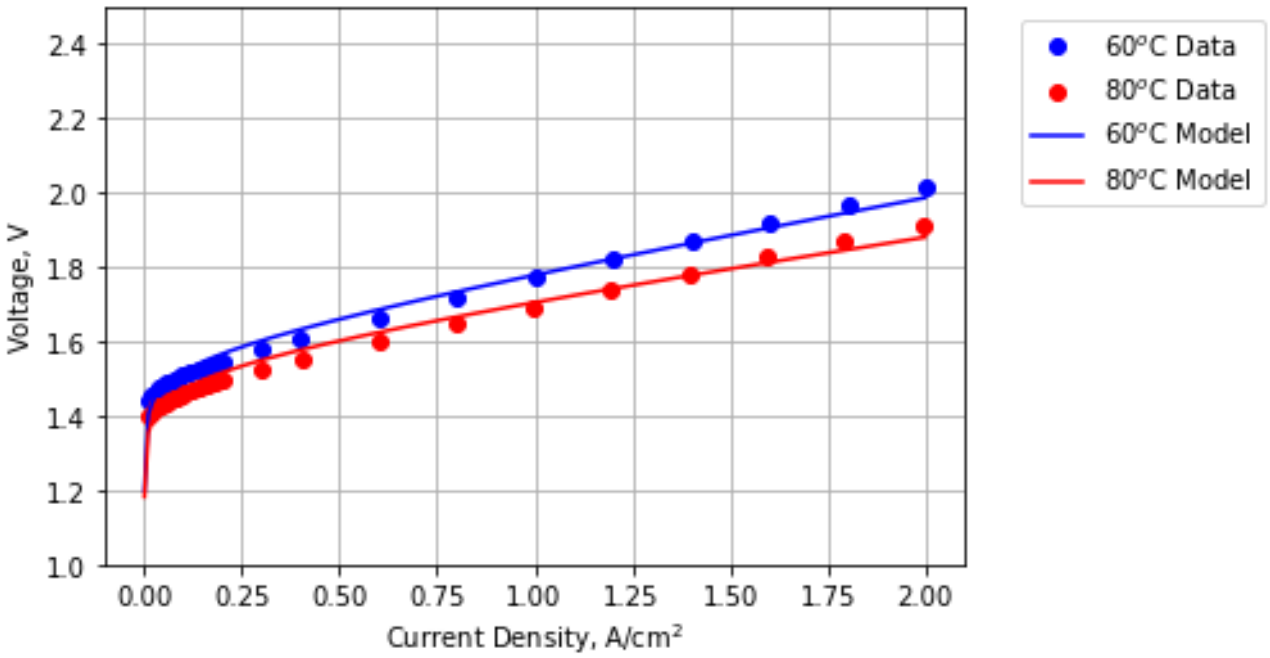

Figure S1: Comparison of the electrolyzer model (line) with experimental data (circles) at 80°C (red) and 60°C (blue) in ambient pressure. Data from [12].

The second experiment is a stack experiment in differential pressure mode. [3] conducted high-pressure experiments with a commercial electrolyzer system from Giner Electrochemical Systems LLC. The stack is made up of twelve cells with an active area of 160 cm^2 each. The experiments were conducted at temperatures between 40 – 55°C and cathode pressures between 1 and 70 bar.

Nafion 110 with a thickness of 254 µm was used in the experiment. In order to match the experimental results, an additional resistance term was added to the model since the resistance from the electrodes, plates, and other wires may no longer be negligible in a stack of 10-15 cells [19]. The values of the model parameters are summarized in Table S5 and Table S6 for the 10-bar-55°C experiment and the 70-bar-40°C experiment, respectively.

Table S5: Electrolyzer Model Parameters for Stack Experiment at 55°C and 10 bar

Parameters	Values	Units
Membrane Thickness, t	254	µm
Electrodes and Plates Resistance, R_{elec}	2.5×10^{-5}	ohms
Cathode Exchange Current Density, $j_{0,cathode}$	1.1×10^{-3} (Calculated)	A/cm^2
Anode Exchange Current Density, $j_{0,anode}$	2.87×10^{-7} (Calculated)	A/cm^2
Temperature, T	55	°C
Cathode Pressure, P_{cat}	10	bar
Anode Pressure, P_{an}	1	bar

Table S6: Electrolyzer Model Parameters for Stack Experiment at 40°C and 70 bar

Parameters	Values	Units
Membrane Thickness, t	254	µm
Electrodes and Plates Resistance, R_{elec}	2.5×10^{-5}	ohms
Cathode Exchange Current Density, $j_{0,cathode}$	0.6×10^{-3} (Calculated)	A/cm^2
Anode Exchange Current Density, $j_{0,anode}$	5.9×10^{-8} (Calculated)	A/cm^2
Temperature, T	40	°C
Cathode Pressure, P_{cat}	70	bar
Anode Pressure, P_{an}	1	bar

Figure S2 shows that the electrolyzer model reasonably matches the experimental results just by changing the operating pressure and temperature while maintaining the rest of parameters the same.

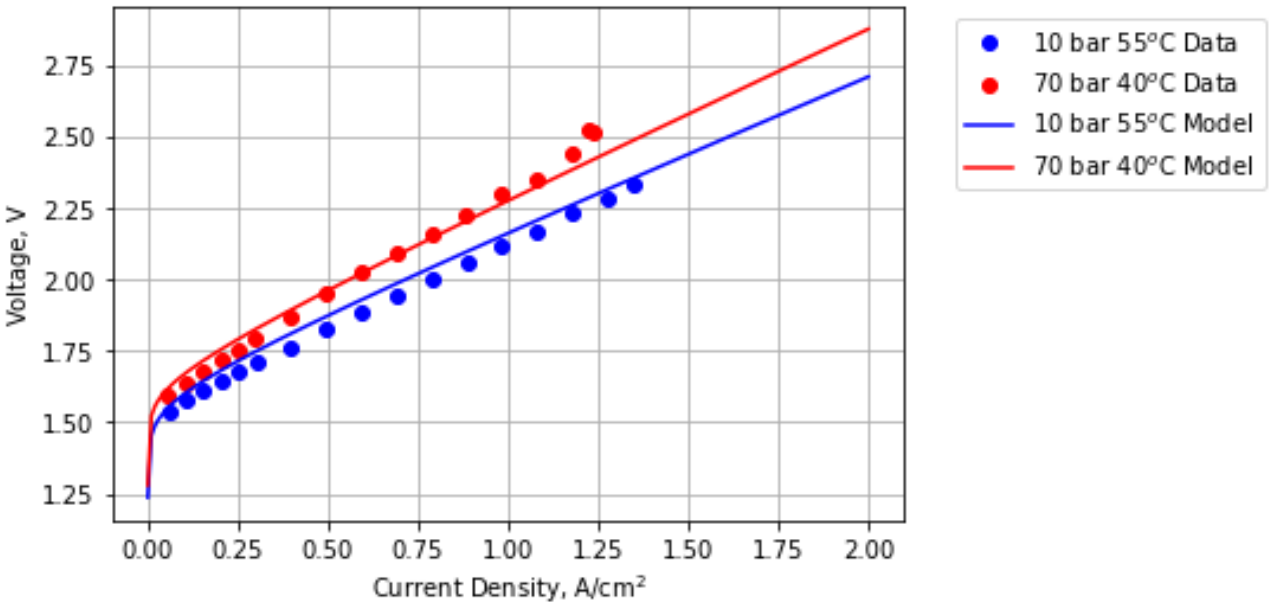

Figure S2: Comparison of the electrolyzer model (line) with experimental data (circles) at (a) 55°C and 10 bar (blue); (b) 40°C and 70 bar (red). Data from (Marangio, Santarelli, and Cali 2009).

For the 2021 and 2035 simulation cases evaluated in this study, the electrolyzer model parameters are configured to reflect the state-of-the-art specifications of the 2021 and 2035 technologies as shown in Table S7.

Table S7: Electrolyzer Model Parameters for 2035 Simulations (IRENA 2020)

Parameters	2021 Scenario	2035 Scenario	Units
Membrane Thickness, t	178	127	µm
Temperature, T	80	80	°C
Cathode Pressure, P_{cat}	30	30	bar
Anode Pressure, P_{an}	1	1	bar
Minimum Current Density	0	0.5	A/cm^2

The 2021 and 2035 polarization curves (red and blue, respectively) are plotted against other benchmark systems from [20] in Figure S3.

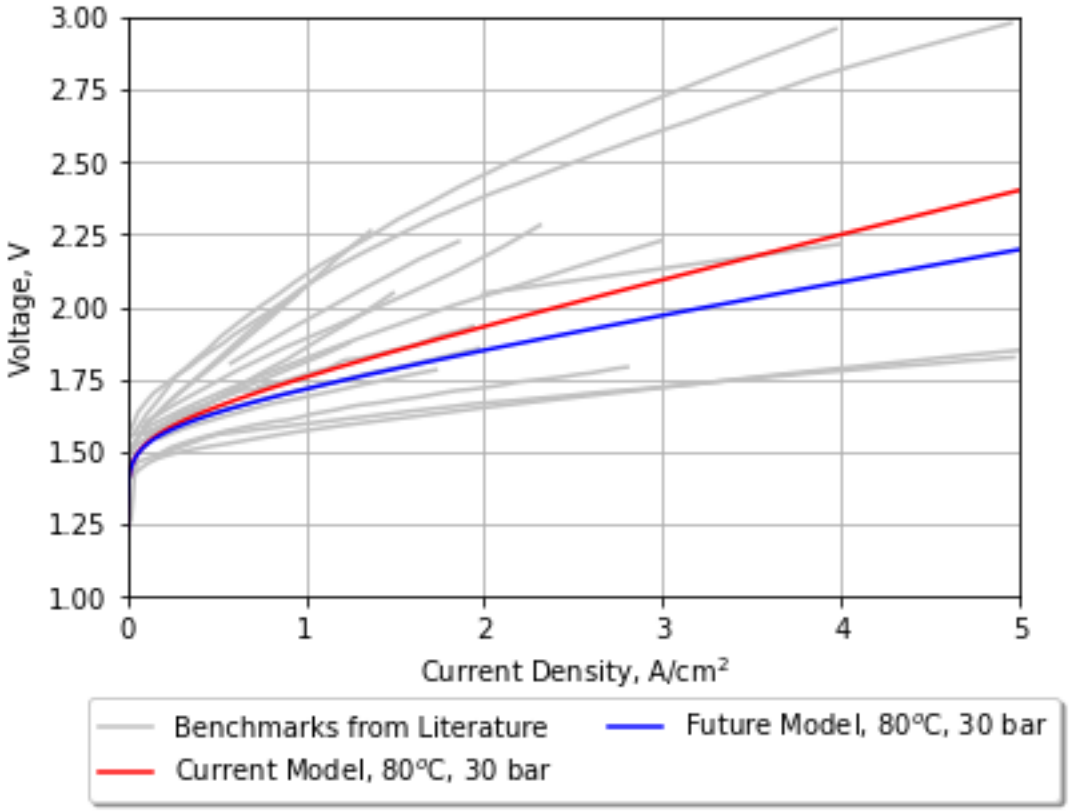

Figure S3: Comparison of the 2021 and 2035 electrolyzer models with other PEM electrolyzer polarization curves from the literature. Benchmark system data from [20].

SI3: Electrolyzer Techno-Economic Model

The electrolyzer techno-economic model uses the discounted cash flow formulation to calculate the present value of all costs associated with planning, permitting, building, and operating the electrolyzer plant. The net present value of the total project cost is calculated by:

$$NPV(C_{Total}) = C_{CAPEX} + C_{storage} + \sum_{y=1}^{40}\left[\left(C_{RP}(y) + C_{fOPEX}(y) + C_{vOPEX}(y)\right)\frac{(1+\pi)^y}{(1+d)^y}\right]$$

(Eq. S16)

The formulation assumes construction in year 0, project start in year 1, a project lifetime of 40 years, a discount rate of 8%, and an annual inflation rate of 1.9%.

The total capital cost, C_{CAPEX}, which is a one-time investment incurred before the plant start-up, is the sum of direct capital, site preparation cost, engineering cost, contingency cost, permitting cost, and land cost. The direct capital is the sum of the capital costs for the electrolyzer stack, mechanical balance-of-

plant, and electrical balance-of-plant. The cost of the mechanical balance-of-plant is proportionally adjusted in accordance with the total hydrogen production capacity of the plant ($/kg H2 per day), whereas the electrical balance-of-plant cost is scaled based on the rated power capacity of the electrolyzer ($/kW). The total stack cost is calculated by multiplying the areal unit cost to the total area of the cells for the plant. In addition, a pressure correction factor to account for additional equipment cost to withstand high-pressure operating conditions was formulated based on industry data from NEL [21], which is shown in S4a. The 15-bar system is approximately 20% more expensive than the ambient system. Assuming that the correction factor increases linearly with operating pressure, a linear correction factor that passes through 1 at 1 bar and 1.2 at 15 bar is constructed, as shown with a red line in S4b. Since the electrolyzer cost model considered here is based on an operating pressure of 300 psi (20.68 bar), the pressure correction factor was normalized by dividing each correction factor by the correction factor at 20.68 bar. The resulting normalized correction factor is also shown with a blue line in S4b. The pressure correction factor ensures that the capital cost for an electrolyzer stack with a 30-bar operating pressure is higher than the cost for an ambient system. Site preparation cost, engineering cost, contingency cost, and permitting cost are expressed as some proportions of the direct capital (2%, 10%, 15%, 15%, respectively) while the land cost is assumed to be fixed (5 acres at $50,000/acre).

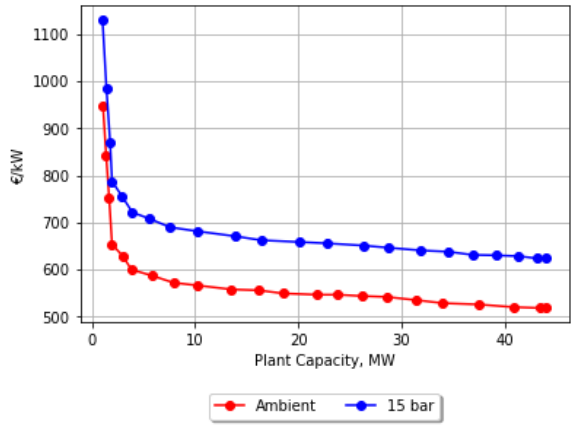

Figure S4a: Capital costs of a 15-bar electrolyzer system (blue) and an ambient pressure electrolyzer system (red) as a function of plant capacity. Adapted from (Saba et al., 2018).

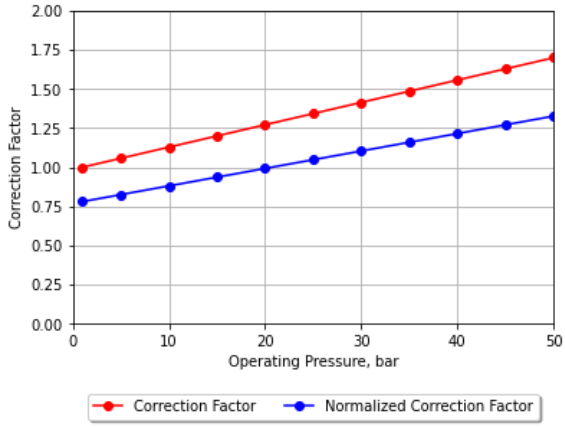

Figure S4b: Original and normalized pressure correction factor as a function of operating pressure from 1 bar to 50 bar.

$C_{storage}$ is the capital cost for a hydrogen storage system, which is assumed at $500 per kg of hydrogen.

The annual replacement cost, $C_{RP}(y)$, is the sum of the planned replacement cost and annual unplanned replacement cost. The planned replacement cost is 15% of the direct capital incurred at a stack replacement interval, which is assumed to be 10 years in this study. The annual unplanned replacement cost, which is 0.5% of the direct capital incurring annually, covers any other miscellaneous part replacements.

The annual fixed operating cost, $C_{fOPEX}(y)$, accounts for the labor cost, overhead cost, tax and insurance cost, and material cost. Labor cost and overhead cost are determined by the number of staff required to operate the plant. Tax and insurance cost is assumed to be 2% of the total capital cost. Material cost is assumed to be 3% of the direct capital.

Finally, $C_{vOPEX}(y)$ is the annual variable operating expense that is made up of electricity cost and water cost. The electricity cost accounts for the amount of power consumed by the electrolyzer stack and the BoPs. The stack power usage is calculated from the polarization curve while the BoP power usage is assumed to be 5.1 kWh kg^{-1} H_2^{-1}. The water cost directly scales with hydrogen production at a consumption rate of 3.78 gallons per kg of hydrogen produced.

SI4: Compression Techno-Economic Model

The compression techno-economic model uses the discounted cash flow formulation to calculate the present value of all costs associated with planning, permitting, building, and operating the mechanical compressors. The net present value of the total project cost is calculated by:

$$NPV\left(C_{Compress}\right) = TCI + \sum_{y=1}^{40}\left[\left(C_{C,OPEX}(y) + C_{C,RP}(y)\right)\frac{(1+\pi)^y}{(1+d)^y}\right] \qquad \text{(Eq. S17)}$$

TCI is the total capital investment of the compressors, which depends on the rated power of the compressor and other factors. For compression in which the inlet pressure (or suction pressure) differs significantly from the outlet pressure (or discharge pressure), multiple compression stages are required to reach the target discharge pressure. The number of compression stages, N, required for high compression ratios (>2) is given by [22].

$$N = \frac{log\left(\frac{P_{disc}}{P_{suc}}\right)}{log(x)} \qquad \text{(Eq. S18)}$$

where P_{disc} is the discharge pressure at the outlet of the compressor, P_{suc} is the suction pressure at the inlet of the compressor, and x is the compression ratio for each stage which is between 2.1 and 4.0. In this study, x is assumed to be 2.1. Compression is typically modeled as an isentropic process and later corrected with an isentropic efficiency factor. For such an ideal multi-stage compression process, the power requirement is given by [22].

$$Power = N\left(\frac{k}{k-1}\right)\left(\frac{Z}{\eta_{isen}}\right)T_{suc}(q_M)R\left[\left(\frac{P_{disc}}{P_{suc}}\right)^{\left(\frac{k-1}{Nk}\right)} - 1\right]$$

(Eq. S19)

where k (1.41 for hydrogen) is the ratio of specific heat under constant pressure (C_p) to specific heat under constant volume (C_v), Z is the average compressibility factor, η_{isen} is the isentropic efficiency, T_{suc} is the suction temperature (usually ambient) at the inlet of the compressor, q_M is the molar flow rate, and R is the universal gas constant. The rated power is calculated by dividing the actual compression power by the motor efficiency, which is assumed as 90% in this study [22].

$$Rated\ Power = \frac{Power}{Motor\ Efficiency}$$

(Eq. S20)

In order to calculate the compressibility factor Z, the average temperature and pressure inside the compression need to be computed. Typically, the suction pressure, the discharge pressure, and the suction temperature are known. Based on the assumptions of an isentropic system, the discharge temperature can be calculated by Eq. S21 [22].

$$T_{disc} = T_{suc}\left[1 + \frac{\left(\frac{P_{disc}}{P_{suc}}\right)^{\left(\frac{k-1}{Nk}\right)} - 1}{\eta_{isen}}\right]$$

(Eq. S21)

The average temperature is given by Eq. S22 [22].

$$T_{average} = \frac{T_{suc} + T_{dis}}{2}$$

(Eq. S22)

The average pressure is given by Eq. S23 [22].

$$P_{avg} = \frac{2}{3}\left(\frac{P_{disc}^3 - P_{suc}^3}{P_{disc}^2 - P_{suc}^2}\right)$$

(Eq. S23)

Finally, Z is evaluated as a function of the average temperature and pressure using the Redlick-Kwong equation of state.

η_{isen} accounts for the non-ideality of the compression process, which is not adiabatic or reversible, and, as a result, some of the work can go into increasing the internal energy or temperature of the system. η_{isen} for large reciprocating compressors range from 65 to 70% while η_{isen} for small reciprocating compressors range from 40 to 50% [22,23]. In this study, an η_{isen} of 65% is assumed [24]. The uninstalled cost (UC) of a compressor scales with the rated power of the compressor. For a high-flow, moderate-compression system, the following scaling factor is applicable [22].

$$UC = 2695.03 \times Rated\ Power^{0.8335} \quad \text{(Eq. S24)}$$

The total installed cost (TIC) of a compressor is calculated by applying an installation factor (IF) to UC:

$$TIC = UC \times IF \quad \text{(Eq. S25)}$$

In this model, the installation factor is assumed to be 2 [22] .

There are other indirect costs associated with the total capital investment (TCI) of a compressor. Site preparation, which is 5% of the TIC, covers the purchase of land and other auxiliary equipment. Engineering and design amounts to 10% of the TIC. Project contingency, which is allocated to deal with any unforeseen issues, takes another 10% of the TIC. Permitting to get the appropriate approvals and control equipment is 3% of the TIC [23]. Finally, the owner's cost, which accounts for the owners' engineering, debt origination, closure costs, and due diligence studies, takes 12% of the TIC [23]. Therefore, the TCI is calculated by adding all these indirect costs to the TIC:

$$TCI = TIC + Indirect\ Costs \quad \text{(Eq. S26)}$$

$C_{C,OPEX}$ is the operating expense, which is made up of the electricity cost, labor cost, overhead cost, and other costs (insurance, property tax, licensing/permits, operating/maintenance/repairs). The electricity cost is calculated based on the hourly hydrogen production rate and the corresponding rate power of the compressor. The labor cost is the product of the labor hours and the hourly labor rate. The required labor hour is given by [22].

$$Labor\ Hour = 288 \times \left(\frac{Daily\ Compressor\ Flow\ Rate}{100{,}000}\right)^{0.25} \quad \text{(Eq. S27)}$$

where $Daily\ Compressor\ Flow\ Rate$ is in kg/day. The average hourly labor rate for 2021 is $42.48/hour (Bureau of Labor Statistics- NAICS code# 2212). The overhead cost is 50% of the labor cost [22]. Insurance, Property Taxes and Licensing and Permits are 1%, 1%, and 0.1% of the TCI. Operating/Maintenance/Repairs costs are 4% of the TIC [22,23]. In addition, the lifetime of a compressor is assumed to be 15 years. Therefore, the compressor needs to be replaced every 15 years. The replacement cost for the compressor is TIC adjusted for inflation.

SI5: Hourly Grid Electricity Prices

18 different electricity forecasts have been used to explore the implications of electricity price variations on future LCOHs. The highlighted traits and assumptions for each forecast is provided in Table S8.

Table S8: Summary of Attributes of 18 Electricity Price Scenarios used in this Study

Forecast Name	Location(s)	Year	Description	Average Price	Number of Hours of <$5MWh	Number of hours of >100/MWh
LAFRESA_6	Southern CA	2021	Historical Locational Marginal Price for the node LAFRESA_6 from CAISO	52.17	258	410
NREL-Mid	Southern CA	2040	Mid-level assumptions for demand, resource, cost, price, technology. No new carbon policy	40.61	222	106
NREL-HighRECost	Southern CA	2040	Mid with 2020 ATB RE advanced projections	44.49	33	106
NREL-LowRECost	Southern CA	2040	Mid with 2020 ATB RE conservative projections	31.78	1584	105
NREL-Mid95by2035	Southern CA	2040	Mid with 95% CO_2 reduction by 2035	59.48	3073	112
NREL-Mid95by2050	Southern CA	2040	Mid with 95% CO_2 reduction by 2050	42	431	109
Princeton-BaseCaseTax	Nationwide	2030	$60/tonne carbon tax, AEO2020 REF natural gas prices, mid cost for all resources	47.69	799	262
Princeton-HighWindTax	Nationwide	2030	BaseCaseTax with low cost for wind clusters	45.06	1628	256
Princeton-HighSolarTax	Nationwide	2030	BaseCaseTax with low cost for solar clusters	45.43	1218	241
NREL-MiNg_$100_CAISO	CA	2035	$100/tonne carbon tax, AEO2020 REF natural gas prices	53.08	3413	518
NREL-MiNg_$150_CAISO	CA	2035	$150/tonne carbon tax, AEO2020 REF natural gas prices	45.54	5080	2702
NREL-MiNg_$100_ERCOT	TX	2035	$100/tonne carbon tax, AEO2020 REF natural gas prices	33.76	4049	79
NREL-MiNg_$150_ERCOT	TX	2035	$150/tonne carbon tax, AEO2020 REF natural gas prices	36.34	5199	1401

Table S8 Continued

Name	Location(s)	Year	Description	Average Price	Number of Hours of <$5MWh	Number of hours of >$100/MWh
NREL-MiNg_$100_MISO-W	AR, IL, IN, IA, KY, LA, MI, MN, MO, MT, ND, SD, TX, WI	2035	$100/tonne carbon tax, AEO2020 REF natural gas prices	35.22	3858	17
NREL-MiNg_$150_MISO-W	AR, IL, IN, IA, KY, LA, MI, MN, MO, MT, ND, SD, TX, WI	2035	$150/tonne carbon tax, AEO2020 REF natural gas prices	28.28	5476	539
NREL-MiNg_$100_NYISO	NY	2035	$100/tonne carbon tax, AEO2020 REF natural gas prices	35.33	4816	185
NREL-MiNg_$150_NYISO	NY	2035	$150/tonne carbon tax, AEO2020 REF natural gas prices	33.84	5834	1421
NREL-MiNg_$100_PJM-W	DE, IL, IN, KY, MD, MI, NJ, NC, OH, PA, TN, VA, WV, DC	2035	$100/tonne carbon tax, AEO2020 REF natural gas prices	48.08	1397	50
NREL-MiNg_$150_PJM-W	DE, IL, IN, KY, MD, MI, NJ, NC, OH, PA, TN, VA, WV, DC	2035	$150/tonne carbon tax, AEO2020 REF natural gas prices	49.94	2666	1903

The profile and short descriptions of each electricity forecast scenario is provided below:

- LAFRESA_6: This is historical locational marginal pricing for the node LAFRESA_6 in Southern California in 2021 obtained from CAISO's database. The average price is $52.17/MWh.

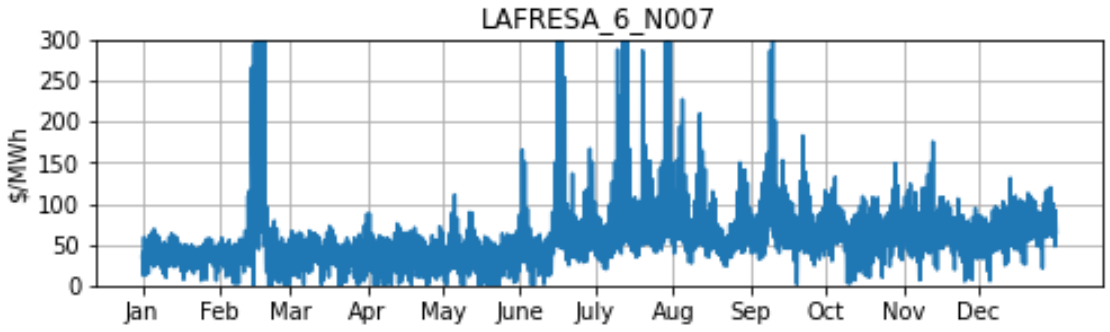

- NREL-Mid: This is NREL's business-as-usual scenario [25]. The 2040 electricity prices from the P10 balancing area (Southern California) were used for this study. The average price is $40.61/MWh. There are spikes of high prices during the summer.

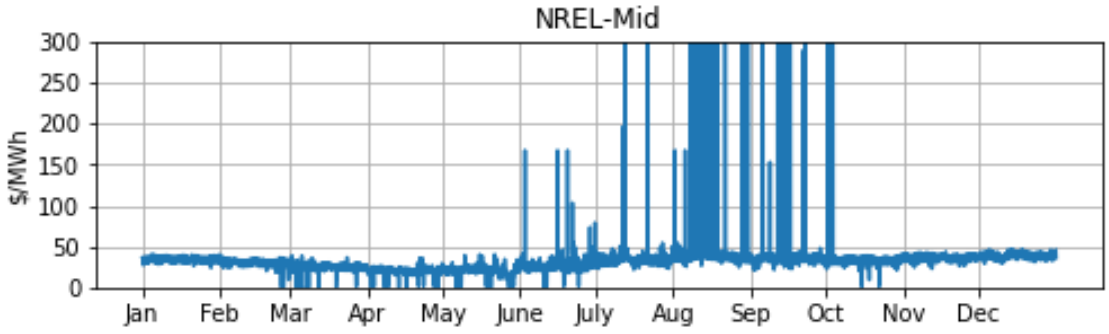

Figure S5: Electricity Price Predictions from NREL-Mid Scenario

- NREL-HighRECost: This 2040 scenario has the same assumptions as NREL-Mid scenario, but with higher renewable energy costs (Gagnon et al., 2021). The electricity prices from the P10 balancing area (Southern California) were used for this study. The average price is $44.49/MWh. There are spikes of high prices during the summer.

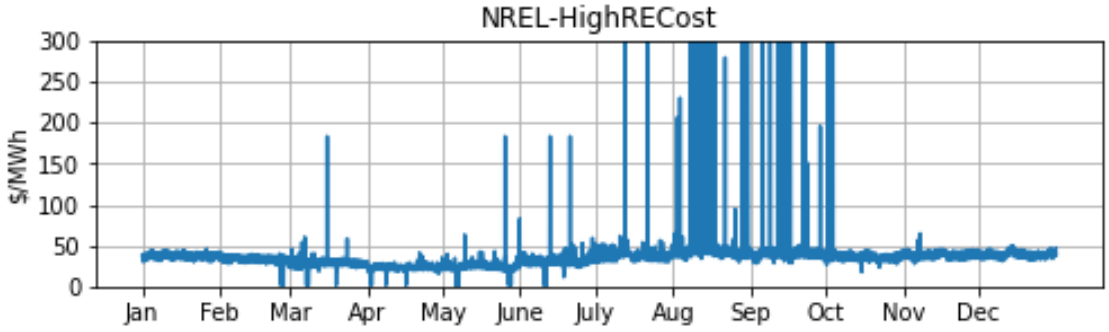

Figure S6: Electricity Price Predictions from NREL-HighRECost Scenario

- NREL-LowRECost: This 2040 scenario has the same assumptions as NREL-Mid scenario, but with lower renewable energy costs [25]. The electricity prices from the P10 balancing area (Southern California) were used for this study. The average price is $31.78/MWh. There are spikes of high

prices during the summer time. Low electricity prices are available during the spring time.

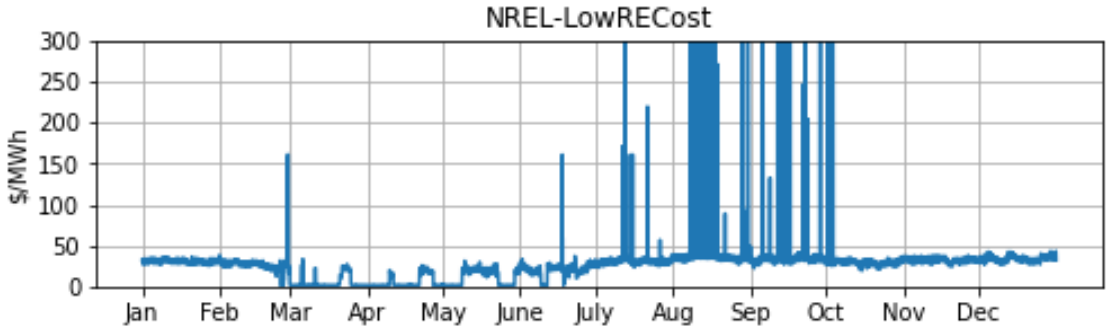

Figure S7: Electricity Price Predictions from NREL-LowRECost

- NREL-Mid95by2035: This 2040 scenario has the same assumptions as NREL-Mid scenario, but with 95% decarbonization of the national power sector by 2035 [25]. The electricity prices from the P10 balancing area (Southern California) were used for this study. The average price is $59.48/MWh with higher levels of fluctuations throughout the day. There are spikes of high prices during the summer. Low electricity prices are available during the spring time.

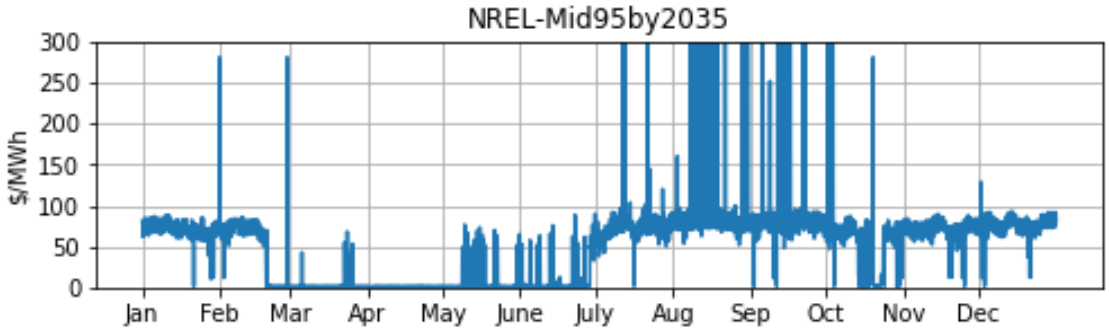

Figure S8: Electricity Price Predictions from NREL-Mid95by2035

- NREL-Mid95by2050: This 2040 scenario has the same assumptions as NREL-Mid scenario, but with 95% decarbonization of the national power sector by 2050 [25]. The electricity prices from the P10 balancing area (Southern California) were used for this study. The average price is $42.00/MWh. There are spikes of high prices during the summer. Highly-fluctuating low electricity prices are available during the spring time.

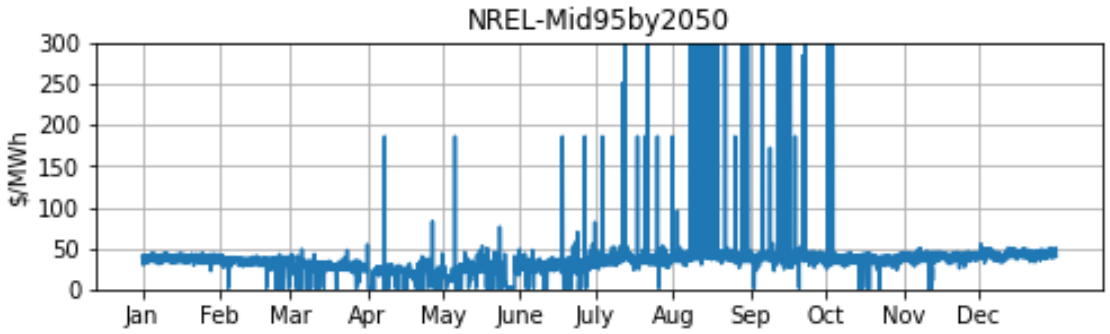

Figure S9: Electricity Price Predictions from NREL-Mid95by2050

- Princeton-BaseCaseTax: This 2030 prediction is based on the US-wide aggregate load and existing capacity with Carbon Tax of $60/tonne [26]. It assumes AEO2020 REF natural gas prices and ATB2020 mid costs for all resources. The average price is $47.69/MWh. There are high fluctuations throughout the year. The prices are generally higher during the summer.

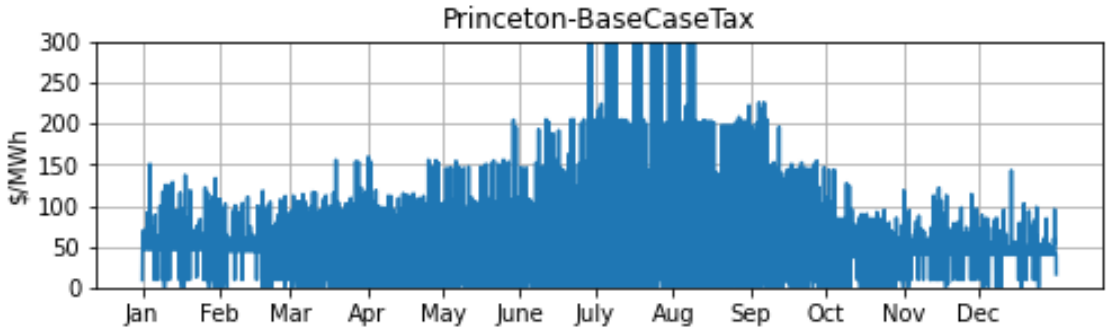

Figure S10: Electricity Price Predictions from Princeton-BaseCaseTax

- Princeton-HighWindTax: This 2030 prediction is based on the US-wide aggregate load and existing capacity with Carbon Tax of $60/tonne [26]. It assumes AEO2020 REF natural gas prices and ATB2020 low costs for new wind clusters. The average price is $45.06/MWh. There are high fluctuations throughout the year. The prices are generally higher during the summer.

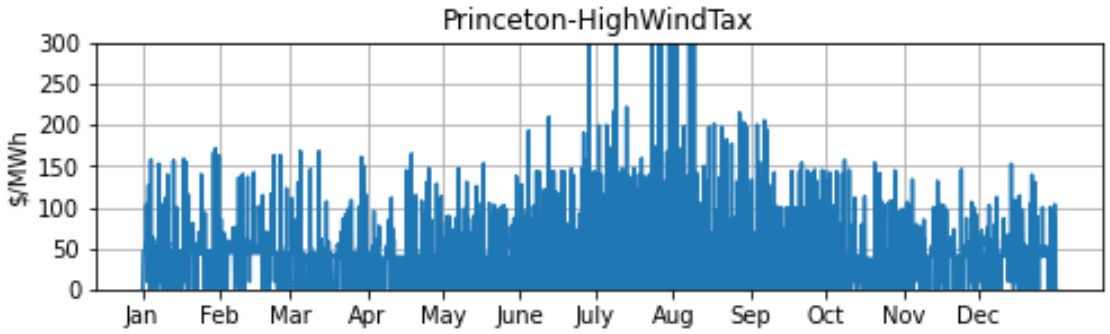

Figure S11: Electricity Price Predictions from Princeton-HighWindTax

- Princeton-HighSolarTax: This 2030 prediction is based on the US-wide aggregate load and existing capacity with Carbon Tax of $60/tonne [26]. It assumes AEO2020 REF natural gas prices and ATB2020 low costs for new solar clusters. The average price is $45.43/MWh. There are high fluctuations throughout the year. The prices are generally higher during the summer.

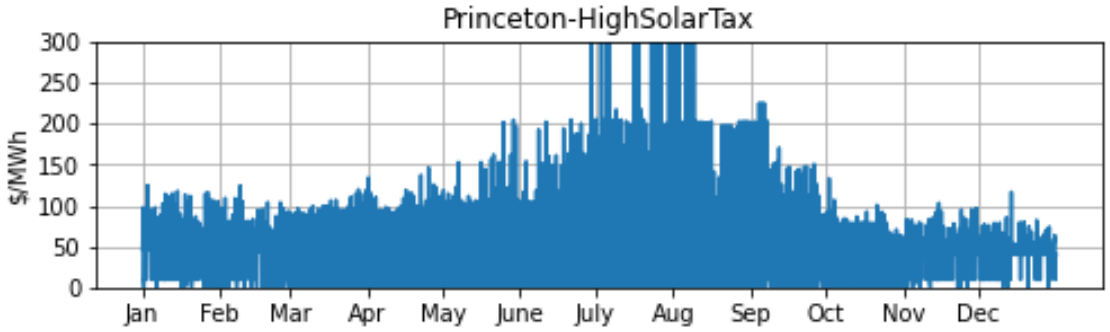

Figure S12: Electricity Price Predictions from Princeton-HighSolarTax

- NREL-MiNg_$100_CAISO: This NREL scenario predicts 2035 electricity prices for California Independent System Operator (CAISO) region based on ATB2020 mid technology costs and AEO2020 reference load projections with carbon tax of $100/tonne [27]. The average price is $53.08/MWh. There are high fluctuations throughout the year. The prices are generally higher during the summer.

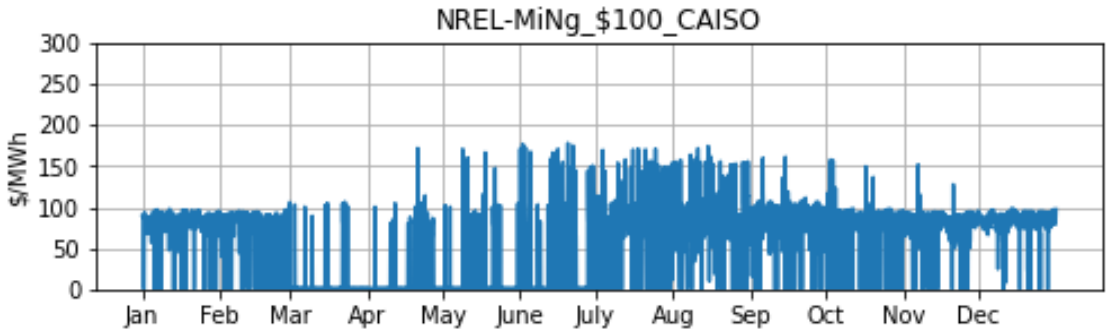

Figure S13: Electricity Price Predictions from NREL-MiNg_$100_CAISO

- NREL-MiNg_$150_CAISO: This NREL scenario predicts 2035 electricity prices for California Independent System Operator (CAISO) region based on ATB2020 mid technology costs and AEO2020 reference load projections with carbon tax of $150/tonne [27]. The average price is $45.54/MWh. There are high fluctuations throughout the year. Low electricity prices are available during the spring time. The prices are generally higher during the summer.

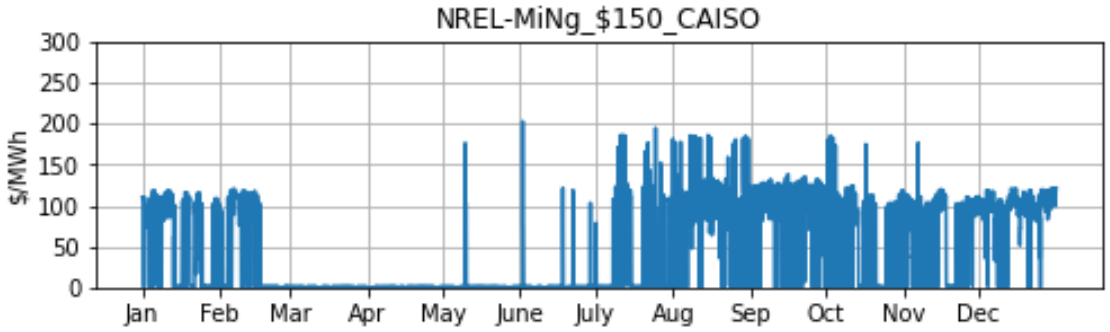

Figure S14: Electricity Price Predictions from NREL-MiNg_$150_CAISO

- NREL-MiNg_$100_ERCOT: This NREL scenario predicts 2035 electricity prices for Electric Reliability Council of Texas (ERCOT) region based on ATB2020 mid technology costs and AEO2020 reference load projections with carbon tax of $100/tonne [27]. The average price is $33.76/MWh. There are high fluctuations throughout the year. Low electricity prices are available during spring time. The prices are generally higher during the summer.

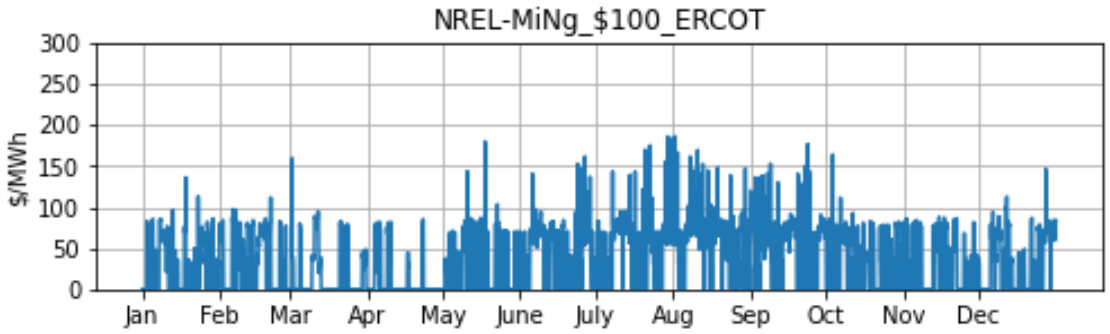

Figure S15: Electricity Price Predictions from NREL-MiNg_$100_ERCOT

- NREL-MiNg_$150_ERCOT: This NREL scenario predicts 2035 electricity prices for Electric Reliability Council of Texas (ERCOT) region based on ATB2020 mid technology costs and AEO2020 reference load projections with carbon tax of $150/tonne [27]. The average price is $36.34/MWh. There are high fluctuations throughout the year. Low electricity prices are available during spring time. The prices are generally higher during the summer.

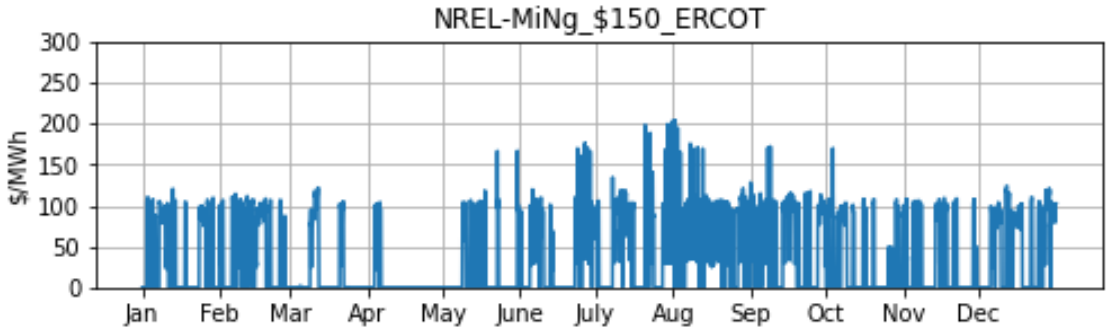

Figure S16: Electricity Price Predictions from NREL-MiNg_$150_ERCOT

- NREL-MiNg_$100_MISO-W: This NREL scenario predicts 2035 electricity prices for Midcontinent Independent System Operator (MISO) region based on ATB2020 mid technology costs and AEO2020 reference load projections with carbon tax of $100/tonne [27]. The average price is $35.22/MWh. There are high fluctuations throughout the year. Low electricity prices are available during the spring time. The prices are generally higher during the summer.

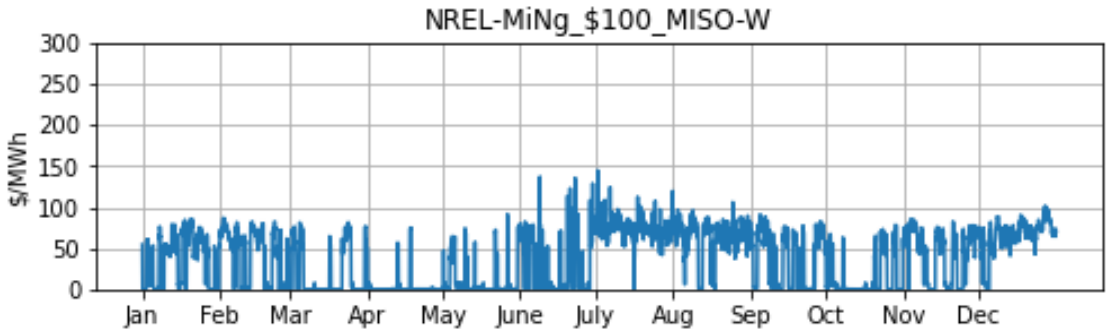

Figure S17: Electricity Price Predictions from NREL-MiNg_$100_MISO-W

- NREL-MiNg_$150_MISO-W: This NREL scenario predicts 2035 electricity prices for Midcontinent Independent System Operator (MISO) region based on ATB2020 mid technology costs and AEO2020 reference load projections with carbon tax of $150/tonne [27]. The average price is $28.28/MWh. There are high fluctuations throughout the year. Low electricity prices are available during the spring and fall. The prices are generally higher during the summer.

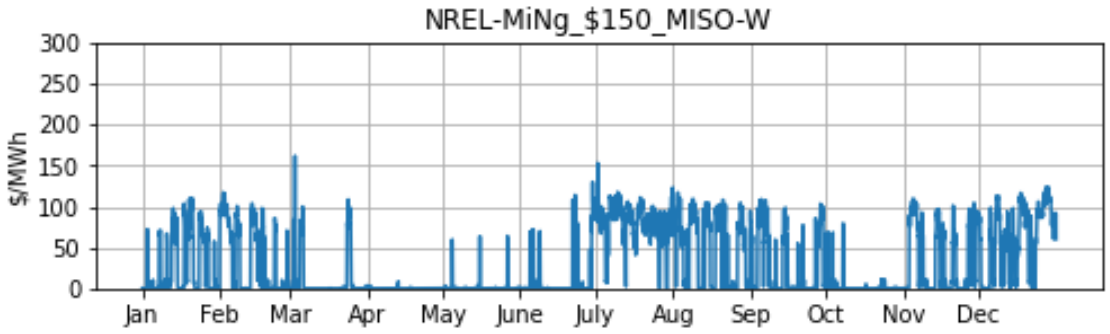

Figure S18: Electricity Price Predictions from NREL-MiNg_$150_MISO-W

- NREL-MiNg_$100_NYISO: This NREL scenario predicts 2035 electricity prices for New York Independent System Operator (NYISO) region based on ATB2020 mid technology costs and AEO2020 reference load projections with carbon tax of $100/tonne [27]. The average price is $35.33/MWh. There are high fluctuations throughout the year. Low electricity prices are available during the spring and fall. The prices are generally higher during the summer.

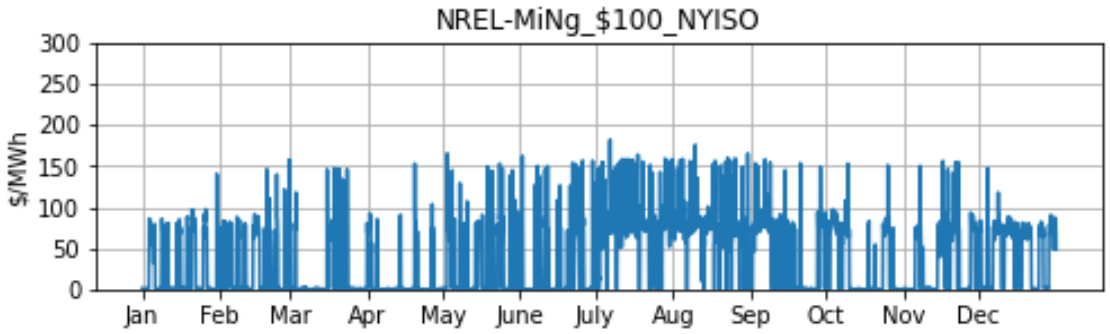

Figure S19: Electricity Price Predictions from NREL-MiNg_$100_NYISO

- NREL-MiNg_$150_NYISO: This NREL scenario predicts 2035 electricity prices for New York Independent System Operator (NYISO) region based on ATB2020 mid technology costs and AEO2020 reference load projections with carbon tax of $150/tonne[27]. The average price is $33.84/MWh. There are high fluctuations throughout the year. Low electricity prices are available during the spring and fall. The prices are generally higher during the summer.

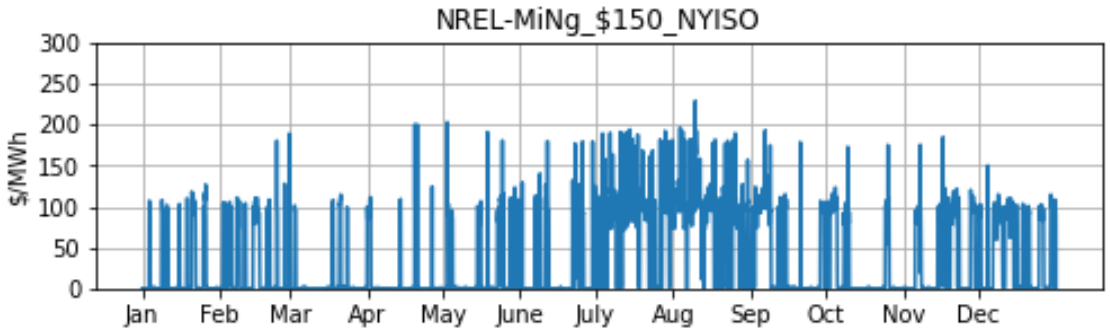

Figure S20: Electricity Price Predictions from NREL-MiNg_$150_NYISO

- NREL-MiNg_$100_PJM-W: This NREL scenario predicts 2035 electricity prices for Pennsylvania-New Jersey-Maryland (PJM) region based on ATB2020 mid technology costs and AEO2020 reference load projections with carbon tax of $100/tonne [27]. The average price is $42.00/MWh. Slightly lower electricity prices are available during the spring. There are spikes of high prices during the summer.

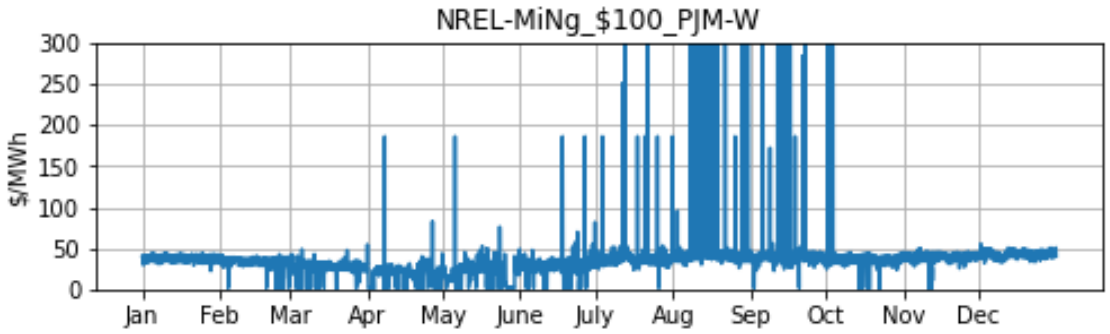

Figure S21: Electricity Price Predictions from NREL-MiNg_$100_PJM-W

- NREL-MiNg_$150_PJM-W: This NREL scenario predicts 2035 electricity prices for Pennsylvania-New Jersey-Maryland (PJM) region based on ATB2020 mid technology costs and AEO2020 reference load projections with a carbon tax of $150/tonne [27]. The average price is $49.94/MWh. There are high fluctuations throughout the year. Low electricity prices are available during the spring and fall. The prices are generally higher during the summer.

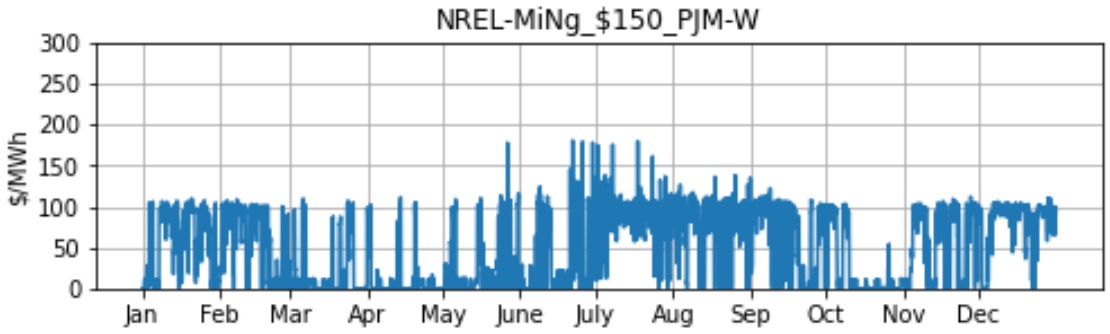

Figure S22: Electricity Price Predictions from NREL-MiNg_$150_PJM-W

SI6: Optimization Model

In order to explore the economic benefits of dynamic operations, an optimization framework is formulated with two objectives: 1) Find the plant capacity that is big enough to allow dynamic operations but not too big to overblow the capital costs; 2) Find the operating current densities that minimize the power usage and the total cost.

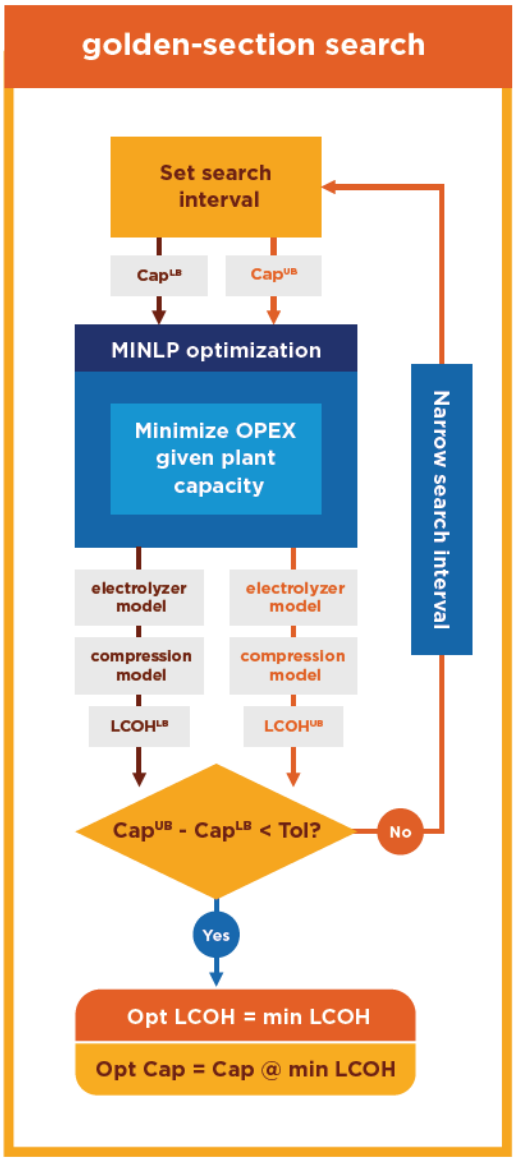

Figure S23: Diagram of the Optimization Framework. The outer-loop Golden-Section Search algorithm (the yellow frame) finds the plant production capacity (tonne/day) that results in the minimum LCOH between an upper bound (UB) and a lower bound (LB) defined by the user. The inner-loop Mixed Integer Non-Linear Programming (MINLP) (the blue box) finds the operating conditions that result in the minimum LCOH for a given plant capacity.

In order to achieve these objectives, the optimization framework utilizes two optimization algorithms, as shown in Figure S23. In the yellow outer-loop, a Golden-Section Search (GSS) algorithm chooses two plant capacities to test, based on the initial search interval. The plant capacities are sent to the blue inner-loop for evaluation. The blue inner-loop uses a Mixed-Integer Non-Linear Programming (MINLP) implemented with Gurobi optimizer to find the operating parameters that result in the minimum LCOH for a given plant capacity. Based on the LCOH values from the two plant capacities, a new search interval is set for the GSS algorithm. If the search interval is less than the desired tolerance level, then the

algorithm terminates and the optimal capacity is set to be the minimum of all the search attempts. Otherwise, the GSS algorithm recursively carries on with the new search interval.

For the MINLP, the electrolyzer techno-economic model is formulated into an optimization problem. The problem is designed to find the operating current density and hydrogen storage size for a given electrolyzer plant size and a target production rate. Hence, the decision variables are as follows:

$$j_{op}(t) = [0, j_{max}] \quad \text{Eq. S28}$$

$$S_{max} \geq 0 \quad \text{Eq. S29}$$

The operating current density at time t , $j_{op}(t)$, has to be greater than 0 and less than or equal to the maximum current density allowed by design. The size of the hydrogen storage tank has to be greater than or equal to 0. The optimization algorithm determines the operating current density at each hour and the storage size that minimizes the net present value of the total cost. Therefore, the objective function can be written as:

$$minimize\ NPV(C_{Total}) = minimize\ C_{CAPEX} + C_{storage} + \sum_{y=1}^{40}\left[\left(C_{PR} + C_{UPR} + C_{fOPEX} + C_{vOPEX}\right)\frac{(1+\pi)^y}{(1+d)^y}\right] \quad \text{Eq. S30}$$

In Eq. S30, C_{CAPEX} stays constant for a given electrolyzer size, which is already determined by the GSS algorithm. $C_{storage}$ increases linearly with the size of storage. The total replacement cost, which is the sum of $C_{PR}(y)$ and $C_{UPR}(y)$, is proportional to the direct capital cost, which stays constant for a given electrolyzer size. Finally, $C_{fOPEX}(y)$ comprises of labor cost, overhead cost, tax and insurance cost, and material cost. Labor and overhead costs are fixed for each calendar year. Tax and insurance cost is proportional to C_{CAPEX}. Material cost is proportional to the direct capital cost. As a result, $C_{fOPEX}(y)$ does not change as a function of the decision variables. Therefore, Eq. S30 can be simplified as:

$$minimize\ C_{storage} + \sum_{y=1}^{40}\left[C_{vOPEX}\frac{(1+\pi)^y}{(1+d)^y}\right] \quad \text{Eq. S31}$$

where

$$C_{storage} = Unit\ Cost\ Factor \times Hydrogen\ Weight\ at\ Capacity \quad \text{Eq. S32}$$

$$C_{vOPEX} = \sum_{d=0}^{364} \sum_{t=24d}^{24(d+1)-1} P_{elec}(t) \times Power_{op}\left(j_{op}(t)\right) + P_{elec}(t) \times U_{elec}^{hourly} \times \dot{m}_{H_2,prod}^{hourly}(t) + P_{water} \times U_{water}^{hourly} \times \dot{m}_{H_2,prod}^{hourly}(t)$$

Eq. S33

The operating power, $Power_{op}(t)$, is a non-linear function of the operating current density, $j_{op}(t)$. For implementation in the Gurobi solver, the non-linear power function is linearized with five piecewise linear functions as shown in Figure S24.

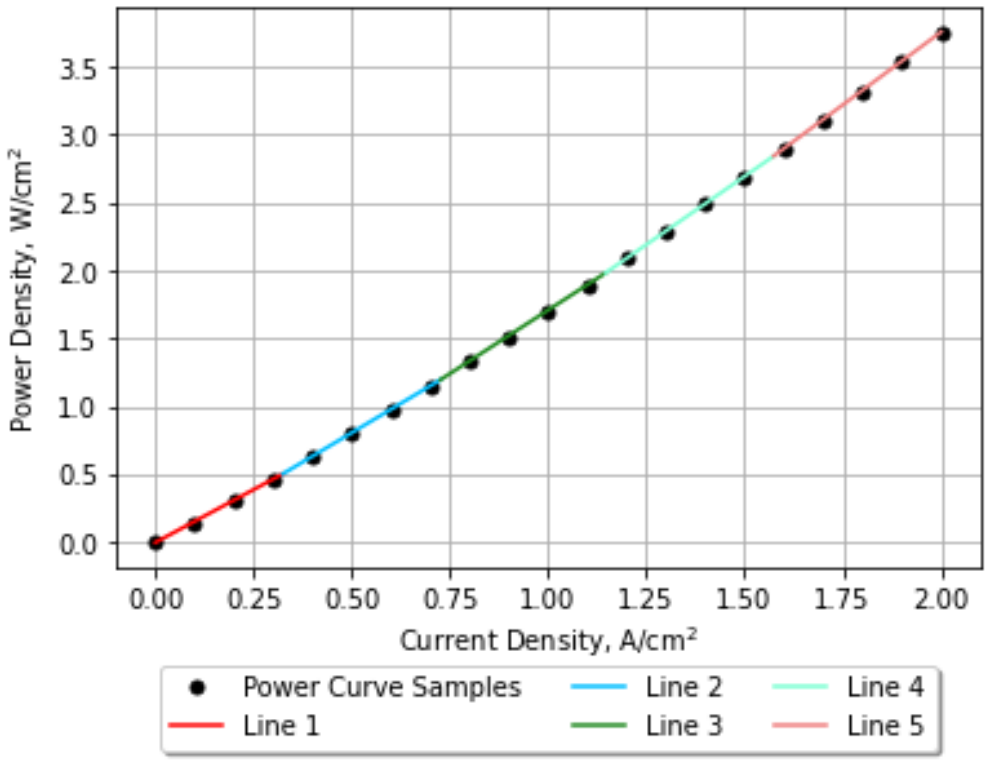

Figure S24: The power curve showing the operating power as a function of current density for a given electrolyzer area. The black dots are sampled data from the electrolyzer model. The colored lines are piece-wise linear functions that are fitted to the model.

Each piecewise linear power function, l, is implemented in the optimization formulation by introducing a binary variable w_l:

$$j_{op}(t) \geq x_{1,l} - M \times \left(1 - w_l(t)\right) \forall\, l = 1,2,3,4,5 \quad \text{Eq. S34}$$

$$j_{op}(t) \leq x_{2,l} + M \times (1 - w_l(t)) \forall\, l = 1,2,3,4,5 \quad \text{Eq. S35}$$

$$Power_{op}(t) \geq Slope_l \times j_{op}(t) + Intercept_l - M \times (1 - w_l(t)) \forall\, l = 1,2,3,4,5 \quad \text{Eq. S36}$$

$$Power_{op}(t) \leq Slope_l \times j_{op}(t) + Intercept_l + M \times (1 - w_l(t)) \; \forall \; l = 1,2,3,4,5 \qquad \text{Eq. S37}$$

$$\sum_{l=1}^{5} w_l(t) = 1 \qquad \text{Eq. S38}$$

Eq. S34 and Eq. S5 activate the linear function that corresponds to the operating current density at each hour. For example, if the current density is 0.25 A/cm^2, then $w_1(t) = 1$ and Line 1 is activated. Eq. S36 and Eq. S37 calculate the power density corresponding to the operating current density. Finally, Eq. S38 ensures that the model is able to pick only one of the five lines for power calculations.

The hourly hydrogen production, $\dot{m}_{H_2}^{hourly}(t)$ in Eq. S39, is directly proportional the operating current density:

$$\dot{m}_{H_2,prod}^{hourly}(t) = \frac{j_{op}(t) \times A}{2F} mole \times \frac{3600\ s}{1\ hr} \times \frac{1\ kg}{1000\ g} \times \frac{2.02\ g}{1\ mole} \qquad \text{Eq. S39}$$

The produced hydrogen can either be stored or exit the system for sales, as shown in Figure S25.

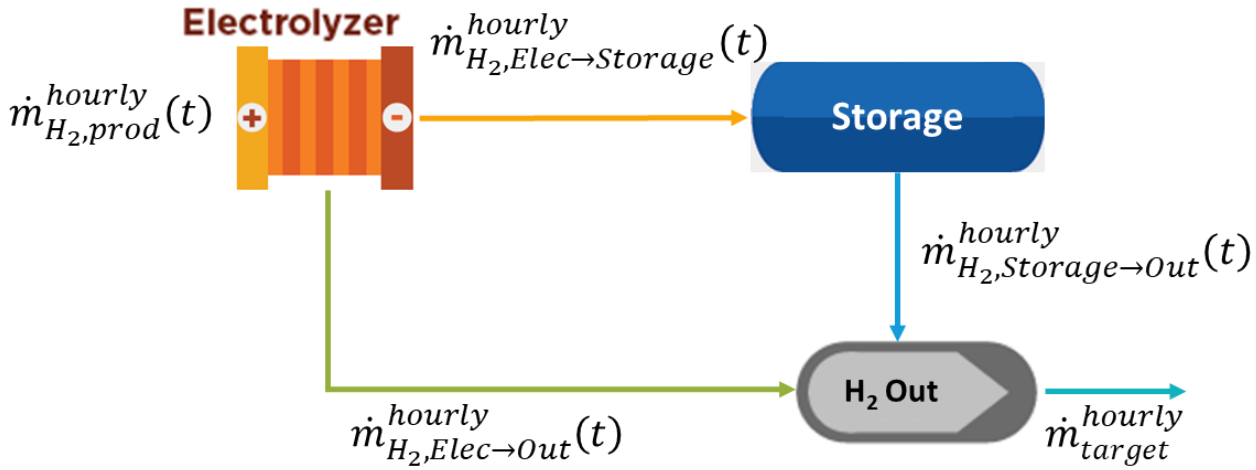

Figure S25: Illustration of hydrogen flow paths from electrolyzer to storage to system outlet.

There is a target amount of hydrogen that needs to be delivered. The demand can be met by production from the electrolyzer and/or discharge from the storage. If it is deemed economical to produce and store excess hydrogen at certain hours (when the electricity is cheap) and discharge it later, the system is allowed to do so. For simplicity, the storage can only be charged or discharged, not both at the same time. These mass balance principles and the charging-discharging dual mode of storage are implemented as follows:

$$\dot{m}_{H_2,prod}^{hourly}(t) \geq \dot{m}_{target}^{hourly} - M \times (1 - ws(t)) \quad \text{Eq. S40}$$

$$\dot{m}_{H_2,prod}^{hourly}(t) \leq \dot{m}_{target}^{hourly} - M \times ws(t) \quad \text{Eq. S41}$$

$$\dot{m}_{H_2,Storage\rightarrow Out}^{hourly}(t) = \left(\dot{m}_{target}^{hourly} - \dot{m}_{H_2,prod}^{hourly}(t)\right) \times (1 - ws(t)) \quad \text{Eq. S42}$$

$$\dot{m}_{H_2,Elec\rightarrow Storage}^{hourly}(t) = \left(\dot{m}_{H_2,prod}^{hourly}(t) - \dot{m}_{target}^{hourly}\right) \times ws(t) \quad \text{Eq. S43}$$

$$\dot{m}_{H_2,prod}^{hourly}(t) = \dot{m}_{H_2,Elec\rightarrow Storage}^{hourly}(t) + \dot{m}_{H_2,Elec\rightarrow Out}^{hourly}(t) \quad \text{Eq. S44}$$

$$\dot{m}_{H_2,Elec\rightarrow Out}^{hourly}(t) + \dot{m}_{H_2,Storage\rightarrow Out}^{hourly}(t) \geq \dot{m}_{target}^{hourly} \quad \text{Eq. S45}$$

Eq. S40 and Eq. S41 are used to determine whether the electrolyzer is producing an excess amount of hydrogen compared to the target rate. Eq. S42 and Eq. S43 ensure that the storage is either in a charging mode or a discharging mode with a binary variable $ws(t)$. Eq. S44 and Eq. S45 ensure the mass balance illustrated in Figure S25.

The storage facility itself is subject to three constraints:

$$S(t) = S(t-1) + \dot{m}_{H_2,Elec\rightarrow Storage}^{hourly}(t) - \dot{m}_{H_2,Storage\rightarrow Out}^{hourly}(t) \; \forall \; t \neq 0 \quad \text{Eq. S46}$$

$$S(1) = S(8760) + \dot{m}_{H_2,Elec\rightarrow Storage}^{hourly}(1) - \dot{m}_{H_2,Storage\rightarrow Out}^{hourly}(1) \quad \text{Eq. S47}$$

$$S(t) \leq S_{max} \quad \text{Eq. S48}$$

Eq. S46 ensures the mass balance for storage. Eq. S47 is a special case of Eq. S46 which requires the system to end with the same storage amount as it started with for each calendar year. Eq. S48 defines the maximum storage capacity, which feeds into the storage capital cost in the objective function (Eq. S31). Additional operating or compression costs associated with storage have not been considered in this study.

Another constraint that is considered in this study is the minimum operating current density limit. For safety and efficiency considerations, there may be a limit to how low the operating current density can drop. In such a case, rather than operating at a current density below the minimum threshold, the electrolyzer should shut down. These constraints are implemented in the model as follows:

$$j_{op}(t) \geq j_{min} - M \times (1 - w(t)) \quad \text{Eq. S49}$$

$$j_{op}(t) \leq 0 + M \times w(t) \quad \text{Eq. S50}$$

Eq. S49 determines whether the operating current density is below the minimum. If so, Eq. S50 sets the operating current density to 0.

In addition, there are non-negativity constraints introduced in the formulation since none of the variables discussed above can be negative in value.

$$j_{op}(t) \geq 0 \quad \text{Eq. S51}$$

$$S(t) \geq 0 \quad \text{Eq. S52}$$

$$\dot{m}_{H_2,prod}^{hourly}(t) \geq 0 \quad \text{Eq. S53}$$

$$\dot{m}_{H_2,Elec\rightarrow Storage}^{hourly}(t) \geq 0 \quad \text{Eq. S54}$$

$$\dot{m}_{H_2,Storage\rightarrow Out}^{hourly}(t) \geq 0 \quad \text{Eq. S55}$$

$$\dot{m}_{H_2,Elec\rightarrow Out}^{hourly}(t) \geq 0 \quad \text{Eq. S56}$$

While the MINLP algorithm looks for the optimal operating current densities and hydrogen storage size to minimize the operating cost and LCOH for a given electrolyzer plant size, the GSS algorithm looks for the optimal plant size that results in the overall lowest LCOH. As shown in Figure S26, the GSS algorithm searches for an extremum of a unimodal function within a specified interval, between a lower bound, x_1, and an upper bound, x_2. It evaluates the function at two different points, x_3 and x_4. The two points are determined such that:

$$\frac{x_2-x_3}{x_3-x_1} = \varphi = \frac{1+\sqrt{5}}{2} \quad \text{Eq. S57}$$

$$\frac{x_4-x_1}{x_2-x_4} = \varphi = \frac{1+\sqrt{5}}{2} \quad \text{Eq. S58}$$

The algorithm looks at the values of $y_3=f(x_3)$ and $y_4=f(x_4)$. If $y_4 > y_3$, then the new search interval is set between x_1 and x_4. If $y_3 > y_4$, then the new search interval is set between x_3 and x_2. The new search interval is shaded in light blue in Figure 5.4 for the two different scenarios. The algorithm continues until the search interval is sufficiently narrowed down to a desired tolerance. The extreme point (minimum in the case shown in Figure S26) is taken as the minimum of all the search iterations that the algorithm performed.

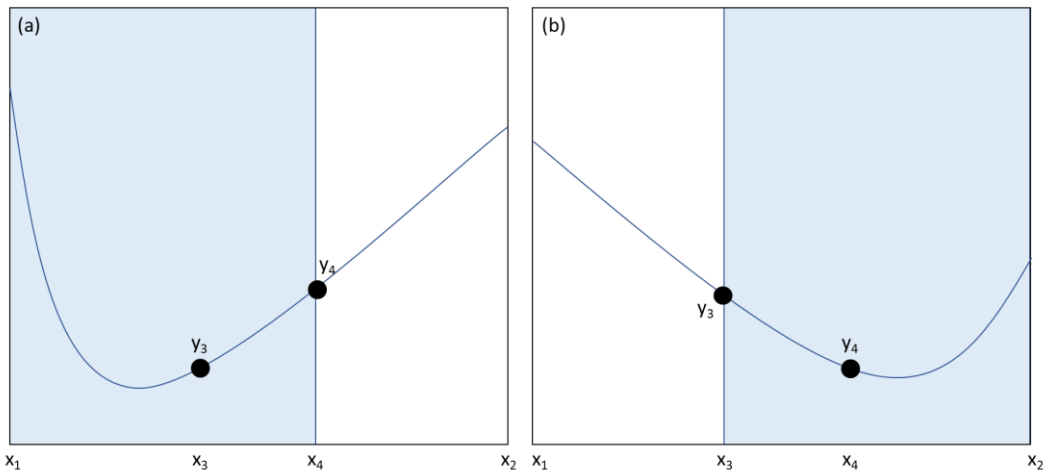

Figure S26: Illustration of how the GSS algorithm works with two unimodal functions with different shapes. In (a), the upper bound of the search interval is updated to x_4 from x_2. In (b), the lower bound of the search interval is updated to x_3 from x_1.

For each dynamic operations scenario, the optimization model produces a result that looks like Figure S27. The green triangle is the LCOH in static operation mode where the electrolyzer capacity is sized to exactly match the demand rate. The blue triangles are the different search iterations that the GSS algorithm evaluated, each triangle representing the solution from the MINLP. The red triangle indicates the lowest LCOH of all cases evaluated. This plot shows that dynamic operations with 40% oversized capacity reduces the LCOH by 9% from $4.93/kg to $4.48/kg.

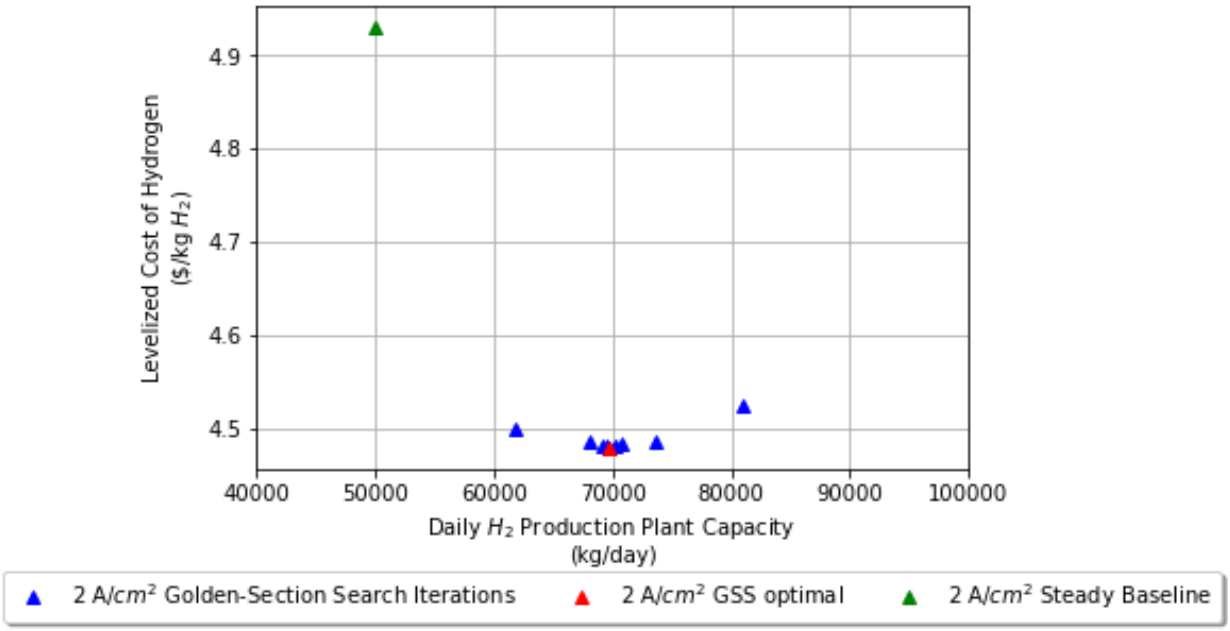

Figure S27: Plot of LCOH as a function of daily production plant capacity with a maximum current density of 2A/cm^2. The blue points are iterations evaluated by the GSS algorithm. The red point is the optimal

case with the lowest total LCOH. The green point is the LCOH from steady operation.

SI7: Emissions Calculation Methodology

The carbon intensity of hydrogen production is assessed by calculating carbon emissions associated with electricity consumption. Based on hourly carbon intensity data for the electricity grid, carbon emissions are computed for each hour by multiplying grid carbon intensity by the electrolyzer power load. Hourly emissions are aggregated over the entire year to quantify total carbon emissions. The carbon intensity of hydrogen is established by dividing total carbon emissions by the mass of hydrogen produced.

$$Hydrogen\ Carbon\ Intensity\ (CI) = \sum_{t=1}^{8760} \frac{Power_{op}(t) \times CI_{grid}(t)}{\dot{m}_{H_2,prod}^{hourly}(t)} \quad \text{Eq. S59}$$

In the assessment of carbon intensity for the 2021 scenario, a seasonal average emissions factor was used for each hour of the day as proposed by CARB[25]. For the future electricity price scenarios, the hourly long-run marginal emissions rate values from the 2021 Cambium dataset were used for the CI calculation[25].

SI8: Low Capital Cost Bookend Case

Previous studies have indicated the potential for electrolyzer CAPEX to decrease to $200/kW with advancements in technology and scaling. To explore the lower bound of the LCOH, a bookend scenario was conducted by assessing the impact of reducing the CAPEX to $200/kW. This was achieved by adjusting the unit cost of the electrolyzer cell to $0.21/cm^2 while maintaining the same BoP costs as in the future scenario models. The $200/kW CAPEX assumption was applied to the scenario with the lowest forecasted LCOH, based on the electricity price forecast for the ERCOT region with a $150/tonne carbon tax (FLECCS MiNg_$150_ERCOT).

Figure S28 illustrates a comparison between two future forecast scenarios based on different CAPEX values: $200/kW and $421/kW. The evident reductions in CAPEX, Replacement Costs, and fixed Operational Expenditure (fOPEX) directly stem from the lowered CAPEX. Additionally, the lower CAPEX scenario benefits from a higher plant capacity (2.4x versus 2.2x), consequently leading to a decrease in variable Operational Expenditure (vOPEX). When summing all cost reductions, it represents a 15% reduction in the Levelized Cost of Hydrogen (LCOH) owing to a 52% reduction in the CAPEX.

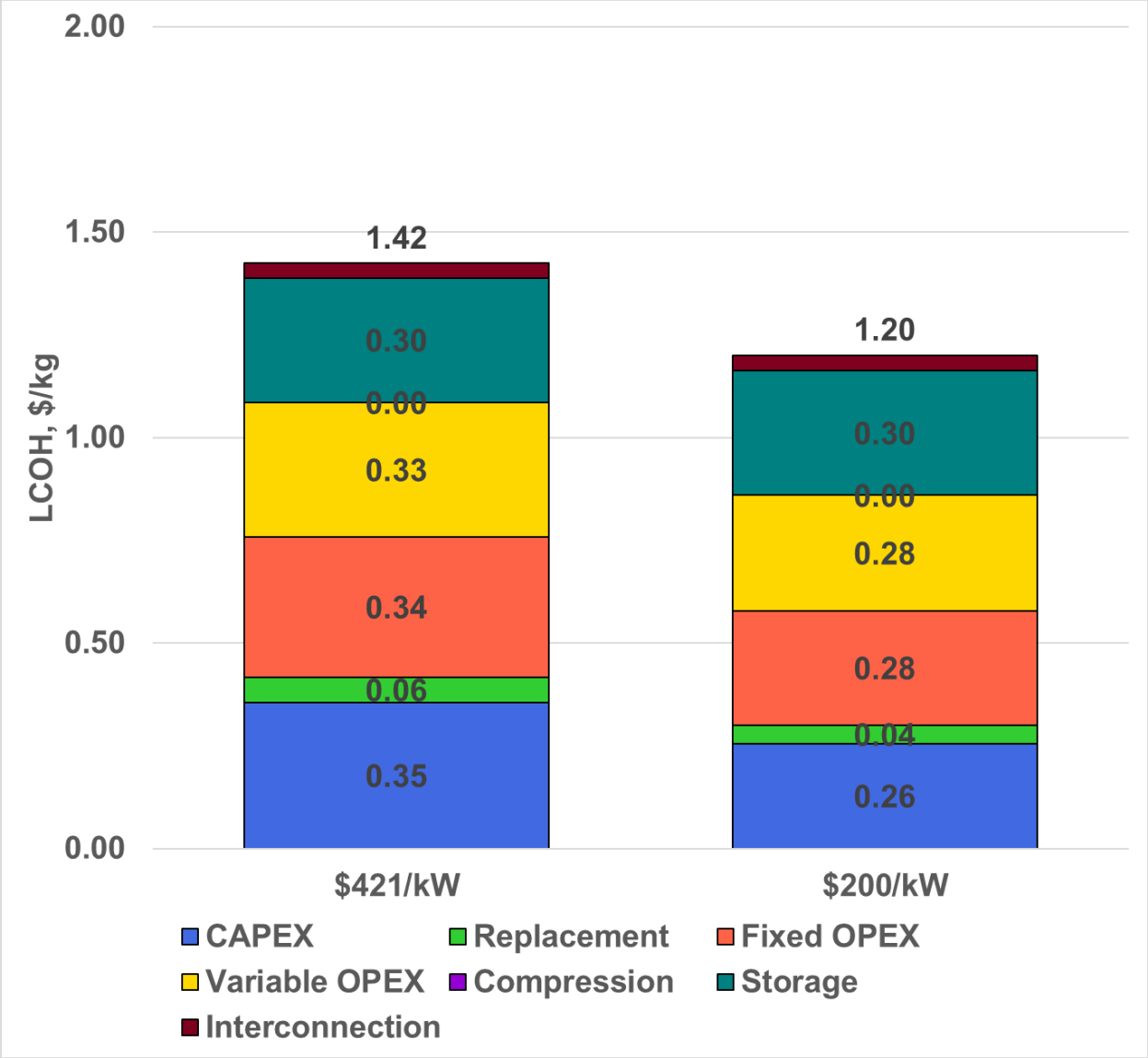

Figure S28: Plot of LCOH for scenarios with $421/kW and $200/kW CAPEX assumptions. FLECCS MiNg_$150_ERCOT is used for the electricity price forecast.

Table S9: Nomenclature for MINLP Optimization Algorithm

A	Total Active Area of the Electrolyzer (cm2)
C_{CAPEX}	Capital Expenditure (CAPEX) ($)
C_{fOPEX}	Fixed Operating Expenses (OPEX) ($)
C_{PR}	Planned Replacement Cost ($)

$C_{storage}$	Storage Cost ($)
C_{Total}	Total Cost ($)
C_{UPR}	Unplanned Replacement Cost ($)
C_{vOPEX}	Variable Operating Expenses (OPEX) ($)
d	Discount Rate (fraction)
F	Faraday's Number (96485.3 C/mol e-)
j_{max}	Maximum Current Density (A/cm2)
j_{min}	Minimum Current Density (A/cm2)
j_{op}	Operating Current Density (A/cm2)
M	"Big M"
$\dot{m}_{H_2,Elec\rightarrow Out}^{hourly}$	Hourly Hydrogen Flow from Electrolyzer to Outlet (kg/hr)
$\dot{m}_{H_2,Elec\rightarrow Storage}^{hourly}$	Hourly Hydrogen Flow from Electrolyzer to Storage (kg/hr)
$\dot{m}_{H_2,Storage\rightarrow Out}^{hourly}$	Hourly Hydrogen Flow from Storage to Outlet (kg/hr)
$\dot{m}_{target}^{hourly}$	Hourly Hydrogen Production Target (kg/hr)
P_{elec}	Electricity Price ($/MWh)
P_{water}	Price of Water ($/gallon)
$Power_{op}$	Operating Power (MW)
S	Hydrogen Storage (tonne)
S_{max}	Maximum Hydrogen Storage Capacity (tonne)
U_{elec}^{hourly}	Hourly Balance of Plant Electrical Usage (kW/hour)
U_{water}^{hourly}	Hourly Water Usage (gallon/kg H_2)
w	Binary Variable for Minimum Current Density
w_l	Binary Variable for Power Function *l*
ws	Binary Variable for Charing-Discharging Mode for Storage
$x_{1,l}$	Lower Limit of Current Density Range for Power Function *l*
$x_{2,l}$	Upper Limit of Current Density Range for Power Function *l*
π	Inflation Rate (fraction)

References

(1) Millet, P. Fundamentals of Water Electrolysis. In *Electrochemical Power Sources: Fundamentals, Systems, and Applications Hydrogen Production by Water Electrolysis*; 2021. https://doi.org/10.1016/B978-0-12-819424-9.00002-1.

(2) Biaku, C. Y.; Dale, N. V.; Mann, M. D.; Salehfar, H.; Peters, A. J.; Han, T. A Semiempirical Study of the Temperature Dependence of the Anode Charge Transfer Coefficient of a 6 KW PEM Electrolyzer. *Int J Hydrogen Energy* **2008**, *33* (16). https://doi.org/10.1016/j.ijhydene.2008.06.006.

(3) Marangio, F.; Santarelli, M.; Calì, M. Theoretical Model and Experimental Analysis of a High Pressure PEM Water Electrolyser for Hydrogen Production. *Int J Hydrogen Energy* **2009**, *34* (3). https://doi.org/10.1016/j.ijhydene.2008.11.083.

(4) Görgün, H. Dynamic Modelling of a Proton Exchange Membrane (PEM) Electrolyzer. *Int J Hydrogen Energy* **2006**, *31* (1). https://doi.org/10.1016/j.ijhydene.2005.04.001.

(5) Abdol Rahim, A. H.; Tijani, A. S.; Kamarudin, S. K.; Hanapi, S. An Overview of Polymer Electrolyte Membrane Electrolyzer for Hydrogen Production: Modeling and Mass Transport. *Journal of Power Sources*. 2016. https://doi.org/10.1016/j.jpowsour.2016.01.012.

(6) Springer, T. E.; Zawodzinski, T. A.; Gottesfeld, S. Polymer Electrolyte Fuel Cell Model. *J Electrochem Soc* **1991**, *138* (8). https://doi.org/10.1149/1.2085971.

(7) García-Valverde, R.; Espinosa, N.; Urbina, A. Simple PEM Water Electrolyser Model and Experimental Validation. *Int J Hydrogen Energy* **2012**, *37* (2), 1927–1938. https://doi.org/10.1016/J.IJHYDENE.2011.09.027.

(8) Bessarabov, D.; Millet, P. *PEM Water Electrolysis*; Pollet, B., Ed.; Academic Press, 2018; Vol. 1.

(9) Ni, M.; Leung, M. K. H.; Leung, D. Y. C. Energy and Exergy Analysis of Hydrogen Production by a Proton Exchange Membrane (PEM) Electrolyzer Plant. *Energy Convers Manag* **2008**, *49* (10). https://doi.org/10.1016/j.enconman.2008.03.018.

(10) Lebbal, M. E.; Lecœuche, S. Identification and Monitoring of a PEM Electrolyser Based on Dynamical Modelling. *Int J Hydrogen Energy* **2009**, *34* (14). https://doi.org/10.1016/j.ijhydene.2009.02.003.

(11) Abdin, Z.; Webb, C. J.; Gray, E. M. Modelling and Simulation of a Proton Exchange Membrane (PEM) Electrolyser Cell. *Int J Hydrogen Energy* **2015**, *40* (39). https://doi.org/10.1016/j.ijhydene.2015.07.129.

(12) Liso, V.; Savoia, G.; Araya, S. S.; Cinti, G.; Kær, S. K. Modelling and Experimental Analysis of a Polymer Electrolyte Membrane Water Electrolysis Cell at Different Operating Temperatures. *Energies (Basel)* **2018**, *11* (12). https://doi.org/10.3390/en11123273.

(13) Escobar-Yonoff, R.; Maestre-Cambronel, D.; Charry, S.; Rincón-Montenegro, A.; Portnoy, I. Performance Assessment and Economic Perspectives of Integrated PEM Fuel Cell and PEM Electrolyzer for Electric Power Generation. *Heliyon* **2021**, *7* (3). https://doi.org/10.1016/j.heliyon.2021.e06506.

(14) Choi, P.; Bessarabov, D. G.; Datta, R. A Simple Model for Solid Polymer Electrolyte (SPE) Water Electrolysis. In *Solid State Ionics*; 2004; Vol. 175. https://doi.org/10.1016/j.ssi.2004.01.076.

(15) Carmo, M.; Fritz, D. L.; Mergel, J.; Stolten, D. A Comprehensive Review on PEM Water Electrolysis. *International Journal of Hydrogen Energy*. 2013. https://doi.org/10.1016/j.ijhydene.2013.01.151.

(16) Coutanceau, C.; Baranton, S.; Audichon, T. Hydrogen Production From Water Electrolysis. In *Hydrogen Electrochemical Production*; 2018. https://doi.org/10.1016/b978-0-12-811250-2.00003-0.

(17) He, Z. Da; Wei, J.; Chen, Y. X.; Santos, E.; Schmickler, W. Hydrogen Evolution at Pt(111) – Activation Energy, Frequency Factor and Hydrogen Repulsion. *Electrochim Acta* **2017**, *255*. https://doi.org/10.1016/j.electacta.2017.09.127.

(18) Suermann, M.; Schmidt, T. J.; Büchi, F. N. Comparing the Kinetic Activation Energy of the Oxygen Evolution and Reduction Reactions. *Electrochim Acta* **2018**, *281*. https://doi.org/10.1016/j.electacta.2018.05.150.

(19) Awasthi, A.; Scott, K.; Basu, S. Dynamic Modeling and Simulation of a Proton Exchange Membrane Electrolyzer for Hydrogen Production. *Int J Hydrogen Energy* **2011**, *36* (22). https://doi.org/10.1016/j.ijhydene.2011.03.045.

(20) Buttler, A.; Spliethoff, H. Current Status of Water Electrolysis for Energy Storage, Grid Balancing and Sector Coupling via Power-to-Gas and Power-to-Liquids: A Review. *Renewable and Sustainable Energy Reviews*. 2018. https://doi.org/10.1016/j.rser.2017.09.003.

(21) Saba, S. M.; Müller, M.; Robinius, M.; Stolten, D. The Investment Costs of Electrolysis – A Comparison of Cost Studies from the Past 30 Years. *International Journal of Hydrogen Energy*. 2018. https://doi.org/10.1016/j.ijhydene.2017.11.115.

(22) Khan, M. A.; Young, C.; Mackinnon, C.; Layzell, D. B. The Techno-Economics of Hydrogen Compression. *Technical Briefs. Canada: Transition Accelerator* **2021**, *1* (1), 1e36.

(23) Chen, T.-P. *Hydrogen Delivey Infrastructure Option Analysis*; 2010.

(24) Parks, G.; Boyd, R.; Cornish, J.; Remick, R. *Hydrogen Station Compression, Storage, and Dispensing Technical Status and Costs: Systems Integration*; 2014.

(25) Gagnon, P.; Frazier, W.; Cole, W.; Hale, E. *Cambium Documentation: Version 2021*; United States, 2021. https://doi.org/10.2172/1835075.

(26) Jesse D Jenkins, S. C. Summary Report of the GenX and PowerGenome Runs for Generating Price Series (for ARPA-E FLECCS Project). Zenodo 2021. https://doi.org/10.5281/ZENODO.5765798.

(27) Cohen, S.; Durvasulu, V. *NREL Price Series Developed for the ARPA-E FLECCS Program*; 2021.